Mon. Not. R. Astron. Soc. **000**, 1–20 (1999) Printed 1 February 2008 (MN LATEX style file v1.4)

Chemo-spectrophotometric evolution of spiral galaxies: II. Main properties of present day disk galaxies

S. Boissier and N. Prantzos
Institut d'Astrophysique de Paris, 98bis, Bd. Arago, 75014 Paris

ABSTRACT

We study the chemical and spectro-photometric evolution of galactic disks with detailed models calibrated on the Milky Way and using simple scaling relations, based on currently popular semi-analytic models of galaxy formation. We compare our results to a large body of observational data on present day galactic disks, including: disk sizes and central surface brightness, Tully-Fisher relations in various wavelength bands, colour-colour and colour-magnitude relations, gas fractions vs. magnitudes and colours, abundances vs. local and integrated properties, as well as spectra for different galactic rotational velocities. Despite the extremely simple nature of our models, we find satisfactory agreement with all those observables, provided the timescale for star formation in low mass disks is longer than for more massive ones. This assumption is apparently in contradiction with the standard picture of hierarchical cosmology. We find, however, that it is extremely successfull in reproducing major features of present day disks, like the change in the slope of the Tully-Fisher relation with wavelength, the fact that more massive galaxies are on average "redder" than low mass ones (a generic problem of standard hierarchical models) and the metallicity-luminosity relation for spirals. It is concluded that, on a purely empirical basis, this new picture at least as successful as the standard one. Observations at high redshifts could help to distinguish between the two possibilities.

Key words: Galaxies: general - evolution - spirals - photometry - abundances

1 INTRODUCTION

Considerable progress has been made in the past ten years or so towards a qualitative understanding of galaxy properties. This has been made in the framework of the Cold Dark Matter (CDM) picture for galaxy formation, either with full N-body simulations coupled to gas hydrodynamics (e.g. Steinmetz 1998) or with simpler, so-called semi-analytic (SAM) models (e.g. Somerville and Primack 1998).

N-body simulations have difficulties up to now in reproducing the observed properties of galaxies in detail. In particular they fail to produce realistic models for present day spirals, because excessive transfer of angular momentum from gas to dark matter results in overly small disks (e.g. Navarro and Steinmetz 1997). Moreover, the first attempt to combine in a single computation dynamical, chemical and photometric evolution (Contardo et al. 1998) failed to reproduce basic observational properties of the Milky Way disk (like the local G-dwarf metallicity distribution or colour gradients at low redshift).

Semi-analytic models, pioneered by White and Frenk (1991) and subsequently augmented by Monte-Carlo methods, were developed by several groups ("Munich": Kauffmann, White and Guiderdoni 1993, Kauffmann 1996, Kauffmann, Nusser and Steinmetz 1997; "Durham": Cole et al. 1994, Baugh et al. 1997; "Santa-Cruz": Somerville and Primack 1998). Such models include a simplified treatment of several essentially unknown ingredients, like star formation, gas cooling, supernova feedback and galaxy merging. They constitute an efficient tool to explore the large parameter space occupied by these (and several other!) unknowns, but they also provide an important level of understanding that could not be achieved by running N-body simulations alone. The successes and shortcomings of such models are nicely reviewed in Somerville and Primack (1998).

Despite the apparent success of SAMs, it is not obvious whether their number of free parameters is smaller than the number of the observables they successfully explain. One rarely mentionned shortcoming is that the assumption of Instantaneous Recycling Approximation (IRA) results in overestimated metallicities and underestimated gas fractions at late times. Moreover, the wealth of available spatial information (i.e. data on gradients of colours, gas and metallicity) as rarely used as constraints to SAMs (with the exception of Kaufmann 1996).

This latter point is dealt with in Jimenez et al. (1998), who use the simple scaling relations for galactic disks (established in the framework of SAMs, see Sec. 2.2) in order to derive initial gaseous profiles. They subsequently calculate the full chemical and spectrophotometric evolution of such disks for the case of Low Surface Brightness (LSB) galaxies and compare succesfully their resulting colour and abundance gradients to observations.

In this paper we adopt an approach similar to that of Jimenez et al. (1998), i.e. we use multi-zone models and simple scaling laws given by SAMs in order to study the evolution of galactic disks. Our method and purpose are, however, different. We calibrate our models to a fairly detailed "template" of the Milky Way (elaborated in a previous paper: Boissier and Prantzos 1999, paper I in this series), while Jimenez et al. (1998) make no such calibration. Moreover, we use a different prescription for the radial dependence of the star formation rate, inspired by theories of star formation in spiral disks (see Sec. 2.1). Finally, we are interested mainly on the properties of High Surface Brightness disks, although (as we shall see) some of our models produce LSBs and some bulges or ellipticals.

Our main objective is to check whether in such an oversimplified framework (i.e. neglecting all the poorly known physics of star-gas interactions, galaxy merging etc.) one can reproduce observations concerning present day disks. For that purpose we use a large body of observational data on disks, concerning sizes and central surface brightness, Tully-Fisher relations in various wavelength bands, colour-colour and colour-magnitude relations, gas fractions vs. magnitudes and colours, abundances vs. local and integrated properties, as well as spectra for different rotational velocities. Comparison of the models to the data turns out to be successfull, provided a crucial assumption is made: that small galaxies form on average their stars *later* than their more massive counterparts. Hierarchical models for galaxy formation produce a radically different picture: low mass objects are generally predicted to form *earlier* than more massive ones and consequently produce older and "redder" stellar populations, contrary to observations. In Somerville and Primack (1998), dust extinction, assumed to be more important in more massive galaxies, is invoked in order to reverse the trend and bring agreement between models and observations. In our models dust extinction plays a minor role, merely enhancing an already correct trend, while at the same time several other observables are naturally reproduced.

The plan of the paper is as follows: In Sec. 2 we present the basic ingredients and the underlying assumptions of the model. The main input parameters and an application to the Milky Way (already discussed in detail in Paper I) are presented in Sec. 2.1. The extension to other galactic disks with the help of simple scaling relations (established in the framework of CDM models) is presented in Sec. 2.2. The assumptions about the infall and star formation rate are discussed in more details in Sec. 2.3. Some results of the models (evolution of the gaseous and stellar content, star formation rate, colour profiles etc.), as well as the main present day properties, are presented in Sec. 3. The results are compared to observations in Sec. 4: disk sizes and central surface brigthness (Sec. 4.1), Tully-Fisher relations in various wavelength bands (Sec. 4.2), colour-colour and colour-magnitude relations (Sec. 4.3), gas fractions vs. magnitudes and colours (Sec. 4.4), abundances vs. local and integrated properties (Sec. 4.5), integrated spectra for different galactic rotational velocities (Sec. 4.6). The results are summarised in Sec. 5, where some comments are also made on the emerging overall picture.

2 THE MODEL

In the previous paper of this series (BP99) we presented a detailed model of the chemical and spectrophotometric evolution of a spiral galaxy and we applied it to the case of the Milky Way disk. In this section, we recall briefly the main ingredients of the model and the results for our Galaxy (Sec. 2.1). Assuming that the Milky Way is a typical spiral galaxy, we extend the model to the study of other spirals, helped by some simple "scaling laws" (Sec. 2.2), which have been established in the framework of the Cold Dark Matter scenarios for galaxy formation. The SFR is then calculated in a self-consistent way, while a further "scaling law" has to be assumed for the infall rate, a crucial ingredient in all realistic models of spiral evolution (see Sec. 2.3).

2.1 Main ingredients and application to the Milky Way

The galactic disk is simulated as an ensemble of concentric, independently evolving rings, gradually built up by infall of primordial composition. The chemical evolution of each zone is followed by solving the appropriate set of integro-differential equations, without the Instantaneous Recycling Approximation. Stellar yields are from Woosley and Weaver (1995) for massive stars and Renzini and Voli (1981) for intermediate mass stars. Fe producing SNIa are included, their rate being calculated with the prescription of Matteucci and Greggio (1986). The adopted stellar Initial Mass Function (IMF) is a multi-slope power-law between 0.1 $M_\odot$ and 100 $M_\odot$ from the work of Kroupa et al. (1993).

The star formation rate (SFR) is locally given by a Schmidt-type law, i.e. proportional to some power of the gas surface density Σ_g: $\Psi \propto \Sigma_g^{1.5}$, according to the observations of Kennicutt (1998); it varies with galactocentric radius R, as:

$$\Psi(t,R) \;=\; \alpha\ \Sigma_g(t,R)^{1.5}\ V(R)\ R^{-1} \qquad (1)$$

where $V(R)$ is the circular velocity at radius R. This radial dependence of the SFR is suggested by the theory of star formation induced by density waves in spiral galaxies (e.g. Wyse and Silk 1989). Since $V(R)$ ∼const. in the largest part of the disk, this is equivalent to $\Psi(R) \propto \Sigma_g(R)^{1.5} R^{-1}$. This latter form of the SFR is used in Prantzos and Silk (1998) and BP99. However, when extending the model to other galaxies with different rotational velocities, we use the form of Eq. (1), and we drop the assumption of $V(R) = const.$ by calculating the full rotation curve (see Sec. 2.3).

The infall rate is assumed to be exponentially decreasing in time, i.e.

$$f(t,R) \;=\; A(R)\ e^{-t/\tau(R)} \qquad (2)$$

with $\tau(R_0{=}8\ \mathrm{kpc}) = 7$ Gyr, in order to reproduce the local G-dwarf metallicity distribution and $\tau(R)$ increasing outwards, from $\tau(R{=}2\ \mathrm{kpc}){=}1$ Gyr to $\tau(R{=}17\ \mathrm{kpc}){=}12$ Gyr

(see Fig. 3). This radial dependence of $f(R)$ is simulating the inside-out formation of galactic disks and, combined with the adopted $\Psi(R)$ allows to reproduce the observed current profiles of gas, oxygen abundance and SFR in the Milky Way disk (see BP99). The coefficient $A(R)$ is obtained by the requirement that at time T=13.5 Gyr, the current mass profile of the disk $\Sigma(R)$ is obtained, i.e.

$$\int_0^T f(t,R) \; = \; \Sigma(R) \tag{3}$$

with $\Sigma(R) \; \propto e^{-R/R_G}$ and a scalelength R_G=2.6 kpc for the Milky Way disk.

The spectrophotometric evolution is followed in a self-consistent way, i.e. with the SFR $\Psi(t)$ and metallicity $Z(t)$ of every zone determined by the chemical evolution, and the same IMF. The stellar lifetimes, evolutionary tracks and spectra are metallicity dependent; the first two are from the Geneva library (Schaller et al. 1992, Charbonnel et al. 1996) and the latter from Lejeune et al (1997). Dust absorption is included according to the prescriptions of Guiderdoni et al. (1998) and assuming a "sandwich" configuration for the stars and dust layers (Calzetti et al. 1994).

This model has several ingredients (stellar yields, tracks, lifetimes, spectra) calculated by the (presumably well understood) theories of stellar atmospheres, evolution and nucleosynthesis, while it has relatively few free parameters. Indeed, we assume that the IMF (obtained by local observations with particular care to the evaluation of the low mass part by Kroupa et al. 1993) and the dependence of the SFR on gas surface density (derived from observations of external spirals, Kennicutt 1998) are not free parameters. On the other hand, the efficiency α of the SFR (Eq. 1) is fixed by the requirement that the local gas fraction $\sigma_g(R_0$=8 kpc)$\sim$0.2, is reproduced at T=13.5 Gyr. We consider then that the really "free" parameters of the model are the radial dependence of the infall timescale $\tau(R)$ and of the SFR; in the latter case, the radial dependence (the $V(R)/R$ factor) has some theoretical motivations (see Wyse and Silk 1989).

The number of observables explained by the model is much larger than the number of free parameters. Leaving aside local observables (age-metallicity relationship, G-dwarf metallicity distribution, O/Fe evolution) the model reproduces present day "global" ones (profiles of gas, O/H, SFR, as well as supernova rates). Moreover, the current disk luminosities in various wavelength bands are successfully obtained along with the corresponding radial profiles; in particular, the adopted inside-out star forming scheme leads to a scalelength of $\sim$4 kpc in the B-band and $\sim$2.6 kpc in the K-band, in agreement with observations (see BP99 for references and details). It is the first time, to our knowledge, that a consistent model for the chemical *and* photometric evolution of the Milky Way is developed. Its success encourages us to extend it to other disk galaxies, in the way described below.

2.2 Scaling properties of disk galaxies

For a simplified description of disk galaxies we adopt here the "scaling properties" derived by Mo, Mao and White (1998, hereafter MMW98) in the framework of the Cold Dark Matter (CDM) scenario for galaxy formation. According to this scenario, primordial density fluctuations give rise to haloes of non-baryonic dark matter of mass M, within which baryonic gas condenses later and forms disks of maximum circular velicity V_C. The mass of the haloes is

$$M \; = \; \frac{V_C^3}{10 \; G \; H(z)} \tag{4}$$

where $H(z)$ is the Hubble parameter at the redshift z of halo formation and G the gravitational constant. The mass of the disk M_d is a fraction m_d of the halo mass

$$M_d \; = \; m_d \; M \tag{5}$$

It is assumed that the disk is thin, rotationally supported and has an exponential surface density profile

$$\Sigma(R) \; = \; \Sigma_0 \; e^{-R/R_d} \tag{6}$$

with central density Σ_0, scalelength R_d and corresponding mass

$$M_d \; = \; 2 \; \pi \; \Sigma_0 \; R_d^2 \tag{7}$$

Eq. (6) describes the initial gaseous profile of the disk; in the terms of our infall model of Sec. 2.1, $\Sigma(R)$ corresponds to the right hand side of Eq. (3). Eqs. (4), (5) and (6) allow to relate the parameters Σ_0 and R_d to an observable, the circular velocity of the disk V_C, but not in a unique way (disks of the same mass M_d and circular velocity V_C may have different Σ_0 and R_d). In order to break the degeneracy one may adopt the spin parameter λ as a second parameter, as e.g. in MMW98. This parameter is related to the halo mass M and angular momentum J through

$$\lambda \; = J \; E^{1/2} \; G^{-1} \; M^{-5/2} \tag{8}$$

where the total energy E of the halo (assumed to be an isothermal sphere) is given by

$$E \; = \; -\frac{M \; V_C^2}{2} \tag{9}$$

Finally, assuming that the angular momentum of the disk

$$J_d \; = \; 2 \; M_d \; V_c \; R_d \tag{10}$$

is a fraction j_d of that of the halo, i.e.

$$J_d \; = j_d \; J \tag{11}$$

one may express the disk parameters Σ_0 and R_d in terms of V_C and λ, as well as j_d, m_d and $H(z)$:

$$R_d \; = \; \frac{1}{10 \; \sqrt{2}} \; \lambda \; V_C \; \left(\frac{j_d}{m_d}\right) \; H(z)^{-1} \tag{12}$$

and

$$\Sigma_0 \; = \; \frac{10}{\pi \; G} \; m_d \; \lambda^{-2} \; V_C \; \left(\frac{j_d}{m_d}\right)^{-2} \; H(z) \tag{13}$$

In this work we ignore the effects of the formation time of the disk, entering Eqs. (12) and (13) through the term $H(z)$. Indeed, it is difficult to incorporate it in the framework of our infall model since the disk is slowly built up and the term "time of formation" has not a precise meaning. We will assume then that all disk galaxies *start forming their stars at the same time (or redshift) and have today the same age as the Milky Way, i.e. T=13.5 Gyr* (notice that the precise formation time is not very important, as far as the corresponding redshift is $z > 3$). We will discuss, however,

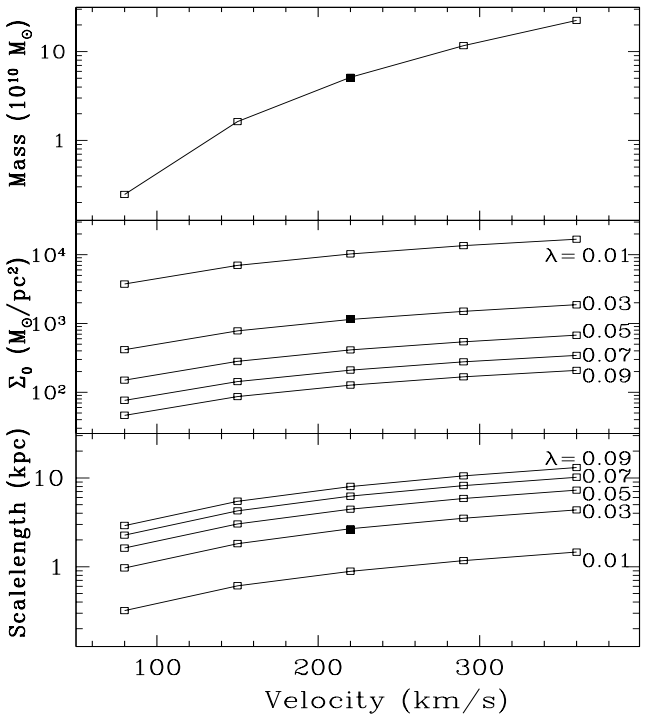

Figure 1. Main properties of our model disks. From top to bottom: mass, central surface density and scalelength, respectively. They are plotted as a function of circular velocity V_C and parametrised with the spin parameter λ. Disk mass depends only on V_C. Filled symbols correspond to the Milky Way model, used for the scaling of all other disks (through eq. 14 and 15, with $m_d = m_{dG}$=0.05).

later the possibility that present day disks have different ages, which is equivalent to assuming different redshifts for their formation.

It is usually assumed that m_d and j_d are constants and, moreover, that j_d/m_d=1, i.e. that the specific angular momentum of the material that forms the disk and the dark halo are the same (see MMW98 and references therein). The latter assumption, although not supported by numerical simulations, simplifies considerably our modelling (otherwise, radial inflows should be induced by angular momentum transfer in the disk, invalidating our model of independently evolving rings). In that case, the profile of a given disk can be expressed in terms of the one of our Galaxy (the parameters of which are designated hereafter by index G):

$$\frac{R_d}{R_{dG}} = \frac{\lambda}{\lambda_G} \frac{V_C}{V_{CG}} \quad (14)$$

and

$$\frac{\Sigma_0}{\Sigma_{0G}} = \frac{m_d}{m_{dG}} \left(\frac{\lambda}{\lambda_G}\right)^{-2} \frac{V_C}{V_{CG}} \quad (15)$$

where we have: R_{dG}=2.6 kpc, Σ_{0G}=1150 M$_\odot$ pc^{-2}, V_{CG}=220 km/s (see BP99 for references on the properties of the Milky Way). Notice that the assumption that all galaxies started forming at the same redshift eliminated $H(z)$ from Eq. 14 and 15. The mass of the disk is M_{dG}=5 10^{10} M$_\odot$ and, assuming m_d=0.05 we obtain M$_G$=10^{12} M$_\odot$ for the mass of the Milky Way's dark halo. Using equs. 5, 8, 9, 10 and 11 one can also evaluate the spin parameter λ as:

$$\lambda = \left(\frac{\sqrt{2}}{G}\right) \left(\frac{m_d}{j_d}\right) R_d\, V_c^2\, M^{-1} \quad (16)$$

Using the above numerical values for the Milky Way (and m_d/j_d=1), we find λ_G=0.03. Eqs. 14 and 15 allow to describe the mass profile of a galactic disk in terms of the one of our Galaxy and of two parameters: V_C and λ. The range of observed values for the former parameter is 80-360 km/s, where for the latter numerical simulations give values in the 0.01-0.1 range, the distribution peaking around $\lambda \sim 0.04$ (MMW98). Although it is not clear yet whether V_C and λ are independent quantities, we treat them here as such and construct a grid of 25 models caracterised by V_C = 80, 150, 220, 290, 360 km/s and λ = 0.01, 0.03, 0.05, 0.07, 0.09, respectively. The corresponding main properties of the disks (mass M_d, central surface density Σ_0 and disk scalelength R_d) appear in Fig. 1, expressed in terms of the adopted parameters V_C and λ. Larger values of V_C correspond to more massive disks and larger values of λ to more extended ones.

As we shall see in Sec. 4.1 the resulting disk radii and central surface brightness are in excellent agreement with observations, except for the case of λ=0.01. We could have excluded that value from our grid on the basis of instability arguments. Indeed, disks dominated by their self-gravity are likely to be unstable to the formation of a bar. According to the discussion in MMW98, for m_d=0.05, this would happen for disks with λ <0.03 (see their Fig. 3). We prefer, however, to keep this λ value in our grid, for illustration purposes; as we shall see, this "unphysical" value leads to the production of galaxies ressembling to bulges or ellipticals, rather than disks.

2.3 SFR and Infall

The two main ingredients of the model, namely the Star Formation Rate $\Psi(R)$ and the infall time-scale $\tau(R)$, are affected by the adopted scaling of disk properties in the following way.

For the SFR we adopt the prescription of Eq. (1), with the same efficiency α as in the case of the Milky Way. In order to have an accurate evaluation of $V(R)$ across the disk, we calculate it as the sum of the contributions of the disk (with the surface density profile of Eq. 6) and of the dark halo, with a volume density profile given by:

$$\rho(R) = \frac{\rho_0}{1 + (\frac{R}{R_C})^2} \quad (17)$$

where ρ_0 is the central density and R_C the core radius (profile on a non-singular isothermal sphere). Other halo profiles (e.g. Navarro et al. 1997) are, probably, more realistic, but their effect on our results is negligible (the resulting rotation curves differ by less than 20% from the one adopted here except in the innermost regions, where spiral waves are less effective and the presence of bulges and bars makes the SFR very uncertain, anyway). The corresponding contributions of the disk and the halo to the rotational velocity are given by (Navarro 1998):

$$V_d(R) = 2\,\pi\,G\,\Sigma_0\,R_d\,x\,[I_0(x)K0(x) - I1(x)K1(x)]^{\frac{1}{2}} \quad (18)$$

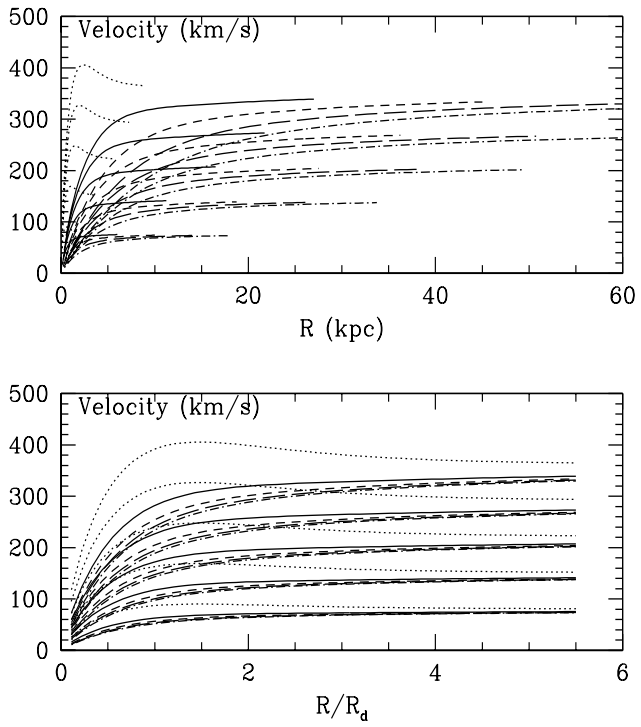

Figure 2. Rotation curves of our disk models as function of radius, expressed in kpc (*upper pannel*) and in disk scalelengths R_d (*lower pannel*). For each of the five values of our grid V_C (80, 150, 220, 290 and 360 km/s) we plot the results for the corersponding five λ values (*dotted* for 0.01, *solid* for 0.03, *short-dashed* for 0.05, *long-dashed* for 0.07 and *dot-dashed* for 0.09).

where $x = R/R_d$ and I_n and K_n are modified Bessel functions of order n ; and

$$V_h(R) \ = \ 4 \ \pi \ G \ \rho_0 \ R_C^2[1 - \frac{R_C}{R} arctan(\frac{R}{R_C})] \qquad (19)$$

respectively, while the final rotation curve is calculated by:

$$V(R)^2 \ = \ V_h(R)^2 \ + \ V_d(R)^2 \qquad (20)$$

The calculated rotation curves for our models appear in Fig. 2, as a function of radius expressed in kpc (*upper pannel*) and in scalelengths R_d (*lower pannel*); it can be seen that in the latter case, a kind of "universal" rotation curve is obtained (excpet for the unrealistic, as we shall see below, λ=0.01 case). Although this velocity profile is not exactly the same as the one derived observationally in Salucci and Persic (1997), it is very close to it and certainly sufficient for the purposes of this work. It allows to calculate the SFR (Eq. 1) in a fully self-consistent way.

The choice of the infall rate $\tau(R)$ is more problematic than the one of the SFR because there are no theoretical principles to guide us. Molla et al. (1999) adopt an exponential radial dependence (with a scale-length of 4 kpc) for $\tau(R)$ in the Milky Way disk and a characteristic time $\tau_0 = \tau_\odot (M_d/M_{dG})^{-1/2}$ for the other galactic disks; this scaling is made on the basis of the association R_{eff}/R_0 (effective radius/solar galactocentric distance) between the Milky Way and the galaxies of their study.

In our case, we have no a priori idea on which region of a given disk will be equivalent to the solar neighborhood.

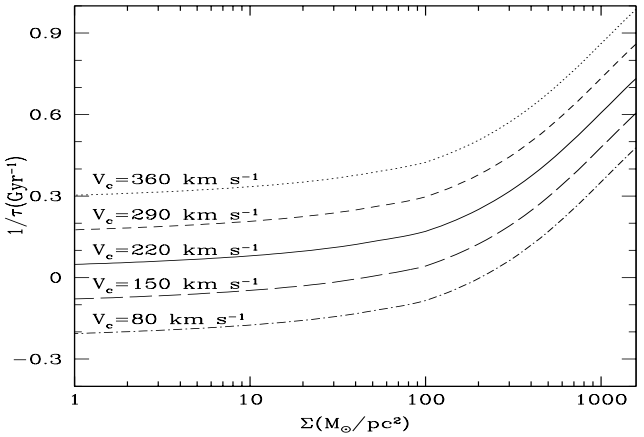

Figure 3. Adopted relation between infall time scale τ and total surface density Σ, generalized from the Milky Way model (*solid curve*) to other galaxies (see Sec. 2.3). Infall is more rapid in denser regions and in more massive galaxies. Negative values of $1/\tau$ mean that the infall rate is increasing in time.

We then adopt the following prescription: the infall time scale increases with both surface density (i.e. the denser inner zones are formed more rapidly) and with galaxy's mass, i.e. $\tau[M_d, \Sigma(R)]$. In both cases it is the larger gravitational potential that induces a more rapid infall. Our adopted infall rate is given by:

$$f[M_d, \Sigma(R), t] \ \propto \ exp\left(-\frac{t}{\tau_G(\Sigma)} + 0.4t\left(1 - \frac{V_C(M_d)}{220}\right)\right) \qquad (21)$$

The corresponding characteristic infall timescales $\tau[M_d, \Sigma(R)]$ appear in Fig. 3, as a function of $\Sigma(R)$ and of V_C. The radial dependence of τ on $\Sigma(R)$ is calibrated on the Milky Way (figure 3) where τ is fixed to 7 Gyr at R_0=8 kpc (to solve the G-dwarf problem) and to 1 Gyr at 2kpc from the galactic center. On the other hand, the mass dependence of τ is adjusted as to reproduce several of the properties of the galactic disks that will be discussed in Sec. 4. The adopted prescription allows to keep some simple scaling relations for the infall in our models and the number of free parameters as small as possible. We recognise that a different parametrisation could be made with a - certainly - non negligible impact on the results. In fact, by suppressing the dependence of τ on galaxy mass (i.e. by assuming the same $\tau[\Sigma(R)]$ relation for all galaxies) we found that several properties of disks - in particular, the colour magnitude and metallicity-luminosity relations - are not well reproduced. The fact that the adopted simple prescription provides a satisfactory agreement with several observed relationships in spirals (see Sec. 4) makes us feel that it could be ultimately justified by theory or numerical simulations of disk formation.

3 MODEL RESULTS

We have computed the chemical and specrophotometric evolution of a grid of 25 disk models (defined by the values of V_C and λ given in Sec. 2.2) up to an age of T=13.5 Gyr. We calculated the evolution of the various chemical and photometric profiles, as well as the disk integrated properties

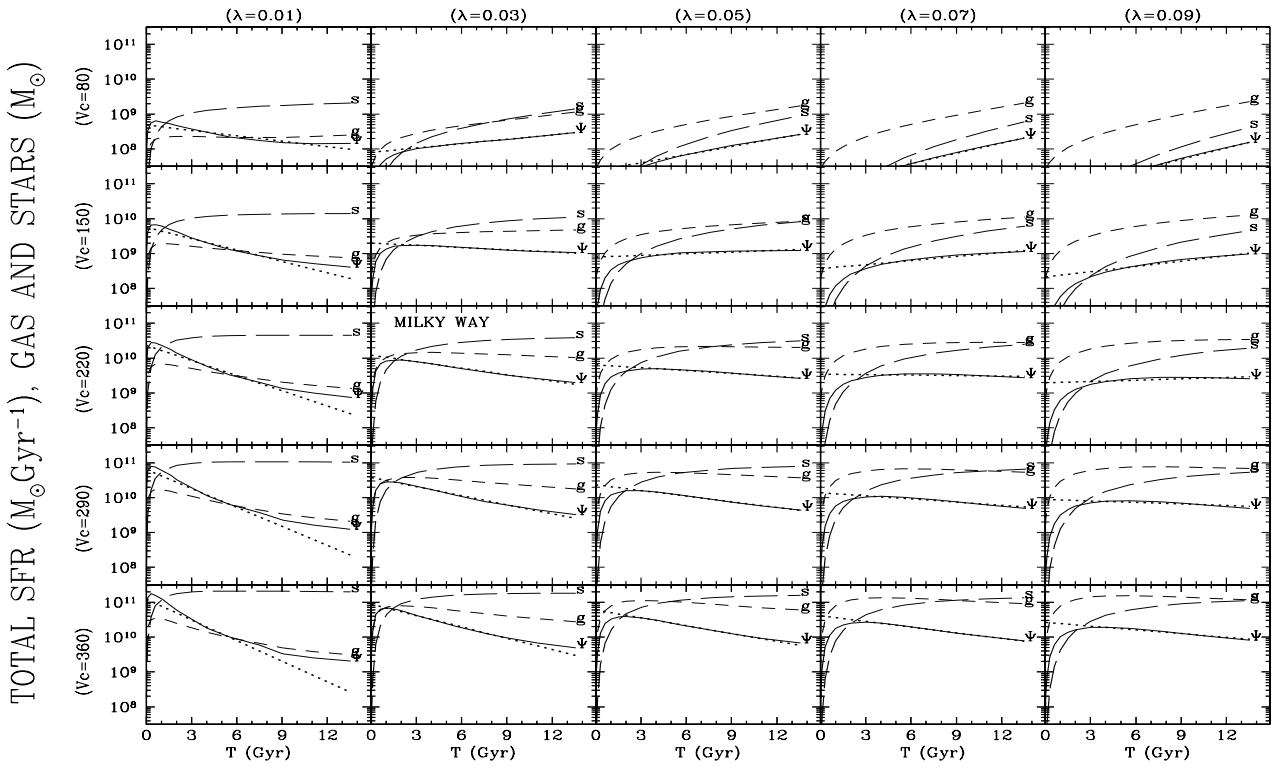

Figure 4. Histories of total SFR (**Ψ**, *solide curve*), gas mass (**g**, *short dashed curve*) and stellar mass (**s**, *long dashed curve*) for our disk models. Each column corresponds to a value of λ and each row to a value of V_C. The *dotted* curve is an exponential fit to the SFR.

according to the procedure outlined in paper I (BP99, Sec. 3.3).

In this work, we concentrate mainly on the integrated properties at T=13.5 Gyr and compare them to observations of local spirals (i.e. at redshift $z \sim 0$, see Sec. 4). However, in this section, we also present some of the results concerning photometric and colour profiles, since their analysis helps to understand the behaviour of the integrated properties and the role of the adopted prescriptions for the SFR and the infall rate. The implications of our models for galaxy observations at higher redshifts, and the corresponding chemical and photometric gradients will be analysed in forthcoming papers.

3.1 Histories of gas, stars and SFR

The evolution of the SFR and of the gaseous and stellar masses in our 25 disk models is shown in Fig. 4. This evolution results from the prescriptions for infall and SFR adopted in Sec. 2.3. Values of SFR range from $\sim$100 $M_\odot$/yr in the early phases of massive disks to $\sim$0.1 $M_\odot$/yr for the lowest mass galaxies. The resulting SFR history is particularly interesting when compared to simple models of photometric evolution, that are usually applied in studies of galaxy evolution and of their cosmological implications. Such models (one-zone, no chemical evolution considered in general) adopt exponentially declining SFR with different caracteristic timescales for each galaxy morphological type

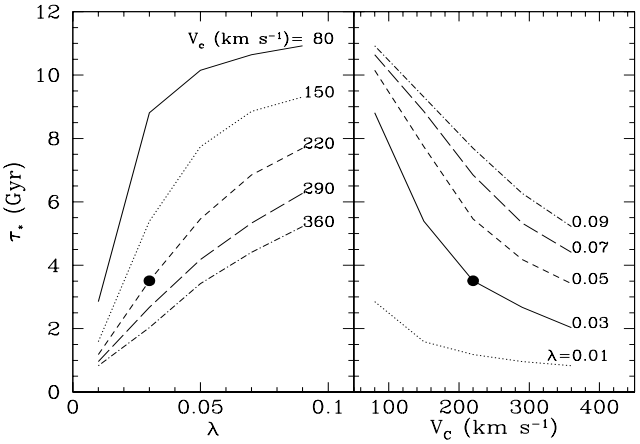

Figure 5. Caracteristic time-scales for star formation, i.e. for forming the first half of the stars of a given galaxy, resulting from our models. They are plotted as a function of the spin parameter λ (*left*) and of circular velocity V_C (*right*). *Filled points* correspond to the Milky Way.

(Guiderdoni & Rocca-Volmerange 1987, Bruzual & Charlot 1993, Fioc & Rocca-Volmerange(1997)).

An inspection of Fig. 4 shows that this may be a relatively good approximation for a large part of galaxy's history, but not for the earliest and latest times (i.e. for the first and last couple of Gyr). We used an exponentially declining

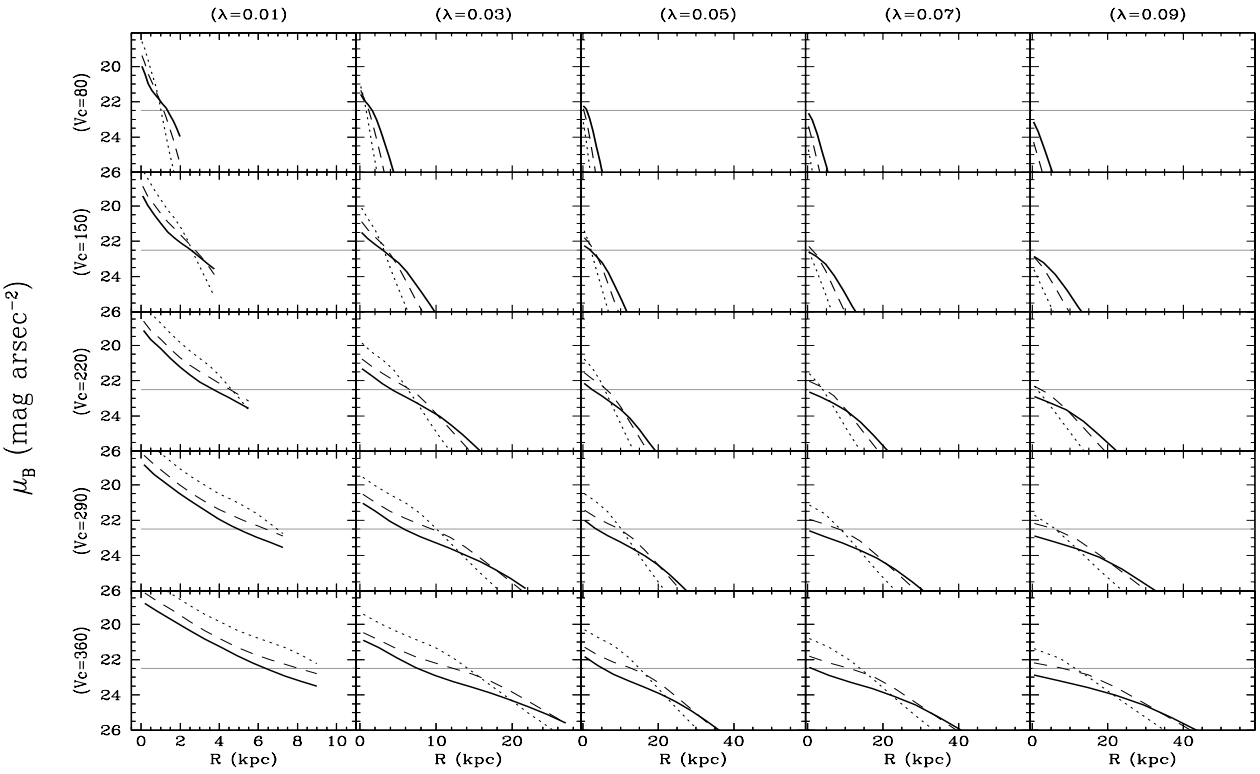

Figure 6. Evolution of the B-band surface brightness profile of our disk models. Profiles are shown at ages T=3 (*dotted*), 7.5 (*dashed*) and 13.5 Gyr (*solid*). The *grey* horizontal line at μ_B=22.5 mag arcsec^{-2} indicates the limit for Low Surface Brightness galaxies. Each column corresponds to a value of λ and each row to a value of V_C (in km/s).

SFR to fit the obtained SFR histories (shown by the dotted curves in Fig. 4). The shortest caracteristic timescales correspond to the more massive and compact disks (larger V_C, smaller λ): in those cases, the rapid infall makes the gas available early on, while the large V_C/R_d factor of the adopted SFR leads to the rapid consumption of that gas. Whether such massive and compact disks exist is another matter (see Sec. 4). As we move to larger values of λ (i.e. more extended disks with larger R_d), the V_C/R_d factor makes star formation less efficient and the resulting SFR has a smoother history. In fact, for most of the values of the parameter couple (V_C, λ) the SFR remains essentially constant during most of the disk's history, since the gas consumption is compensated by the infall. Finally, in the case of the most extended and less massive galaxies (low V_C, large λ) the SFR and gas mass actually increase in time, due to the adopted prescription for infall (which is very slow for low mass and low surface density galaxies). Extended galaxies are found to have low surface brightness (as already shown in Jimenez at al. 1998) and high gas fractions (see Sec. 3.2). In summary, it turns out that λ *affects mainly the shape of star formation history (i.e. the caracteristic time scale of star formation), while* V_C *determines the absolute values of SFR, gaseous and stellar content* (see Sec. 3.4).

The fact that in some cases the SFR increases in time leads us to define the time-scale τ_*, required for forming the first half of the stars of a given galaxy. This time scale for star formation appears in Fig. 5, plotted as a function of λ (left) and V_C (right). It can be seen that τ_* is a monotonically increasing function of λ and a decreasing function of V_C. For the Milky Way (V_{CG}=220 km/s, λ_G=0.03) we find τ_* ∼3.5 Gyr. For galaxies less massive than the Milky Way and $\lambda > 0.06$, it takes more than half the age of the Universe to form the first half of their stars.

3.2 Photometric profiles

In this section we present some results on the photometric evolution of our disk models. We illustrate this evolution by commenting only on the B-band surface brightness profile. Other photometric bands present similar trends and are not shown here, for lack of space; results concerning some of them will be presented in Sec. 4, where comparison is made to a large body of observational data.

The evolution of the B-band surface brightness is shown in Fig. 6 for three ages: t=3, 7.5 and 13.5 Gyr, respectively. It reflects clearly the adopted scheme of inside-out star formation, i.e. the fact that gas is more rapidly available in the inner galactic regions (because of the adopted infall timescale $\tau(R)$), where it is efficiently turned into stars (because of the V/R dependence of the SFR). At late times, relatively little gas is left in the inner regions, but quite a lot is still infalling in the outer ones, maintaining an important SFR there. Several interesting features should be noticed:

a) The central surface brightness μ_{B0} today depends little on V_C, while the more compact (higher λ) disks have,

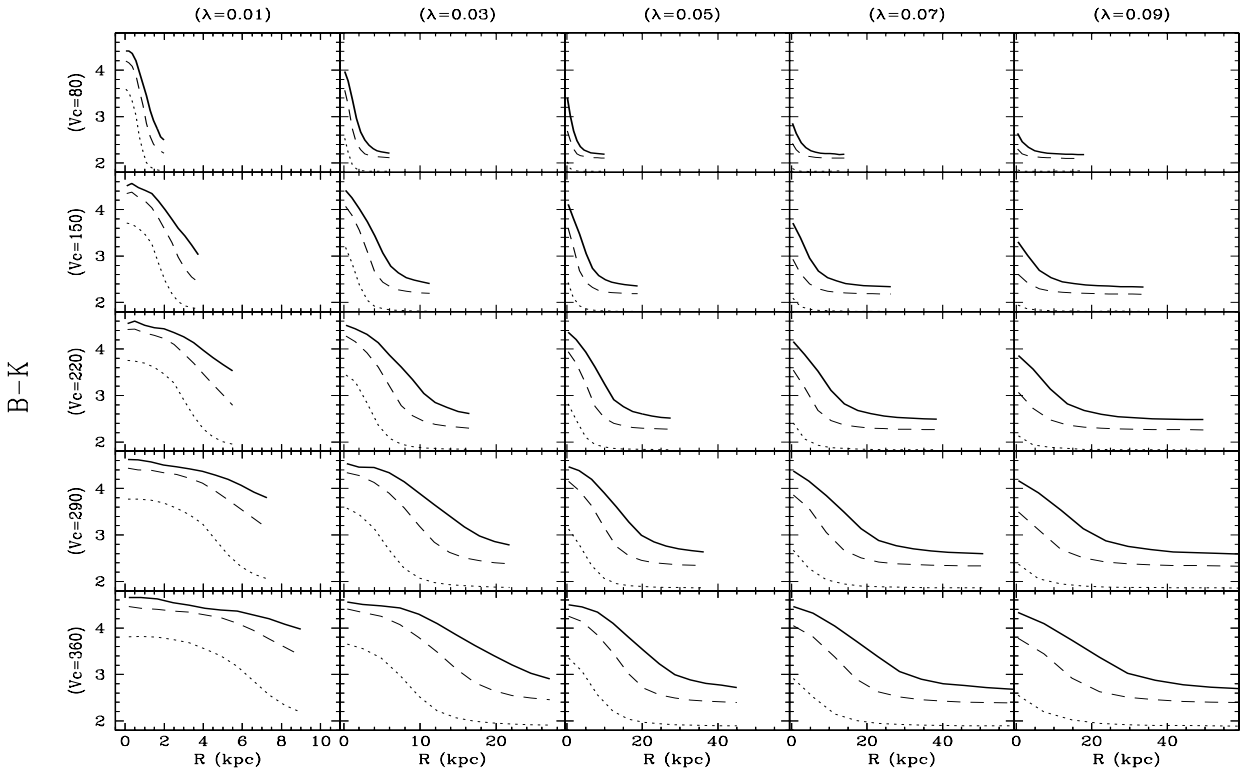

Figure 7. Evolution of the B-K profile of our disk models. Profiles are shown at ages T=3 (*dotted*), 7.5 (*dashed*) and 13.5 Gyr (*solid*). Each column corresponds to a value of λ and each row to a value of V_C (in km/s). Colour profiles generally flatten with time, because of the inside-out scheme of star formation adopted (see text).

in general, higher μ_{B0}. In almost all cases μ_{B0} was higher in the past

b) As a result of the inside-out star formation, the B-band surface brightness profile flattens, in general, with time. Disks were more compact in the past.

c) Photometric profiles are rarely "purely exponential"; indeed, they may deviate considerably from the usually adopted exponential ones. This is in agreement with the conclusions of Courteau and Rix (1999) who find that only about 20% of their sample of more than 500 disk galaxies qualify as pure exponentials.

d) Because of the inside-out star formation scheme, the isophotal radius R_{25} (the radius at which μ_B=25 mag arsec^{-2}) generally increases with time (except for the λ=0.01 case). Present day values of R_{25} in our models are found to range from a few kpc to ∼40 kpc.

e) Several of the models in Fig. 6 have μ_{B0} <22.5 mag arcsec^{-2} at present, i.e.they correspond to Low Surface Brightness (LSB) galaxies. This concerns all the galaxies with λ=0.09 and some with λ=0.07. However, according to our models, some of those galaxies have always been LSBs and some of them not. In the former class belong the less massive galaxies, which were fainter in the past because of their continuously increasing SFR (Fig. 4). In the latter class belong more massive galaxies, which have a declining SFR and therefore were brighter in the past; they became LSBs only after a certain age. Finally, in some intermediate cases (e.g. V_C=150 km/s and λ=0.05, 0.07) the central SFR and corresponding μ_{B0} have remained virtually unchanged during the galaxy's lifetime. These results may have important implications for the study of LSBs as we shall see in Sec. 3.4.

3.3 Colour profiles

Figure 7 presents the evolution of the B-K profiles of our model disks. Again, the SFR histories of Fig. 4 and the inside-our star formation scheme allow to understand the main features:

i) The more compact and more massive a galaxy is, the larger is the final B-K value, either the central (Fig. 7) or the integrated one (Fig. 8). This is due to the fact that low λ and high V_C values favour a rapid early star formation and the existence of relatively old stellar populations today. In fact, the properties of λ=0.01 galaxies correspond more to those of bulges or ellipticals than disk galaxies.

ii) B-K values are always larger in the inner galactic regions, since stars are formed earlier there than in the outer disks. As time goes on, a "reddening" wave propagates outwards in the disks.

iii) More massive disks have a flatter B-K profile than less massive ones with the same λ.

iv) The outer galactic regions have, in general, a "flat" B-K profile, because they form stars at late times. Stellar populations in those regions have, on the average, the same age (they are young) and same B-K values. On the other

hand, in the inner regions there are substantial discrepancies in the timescales of star formation, and colour gradients are consequently established.

v) For a given V_C the final B-K profile is flatter in more compact disks, since the $1/R$ factor of the SFR and the infall timescales are such that efficient early star formation may take place even in their outer regions.

The results presented in the previous section and in this one may have interesting implications for LSB galaxies. Indeed, it can be seen in Figs. 5 and 6 that disks with the same μ_{B0} today may have quite different central colours. This is e.g. the case for ($\lambda = 0.07, V_C$=80 km/s) and ($\lambda = 0.07, V_C$=220 km/s). They both have μ_{B0} ∼23 mag arscec^{-2}, but the former has (B-K)$_0$=2.8, while the latter has (B-K)$_0$=4. This is due to their different SFR histories, since in the former case most of the stars are formed late, while in the latter they are formed quite early on. These results could be related to the conclusions of a recent study by Bell et al. (1999), who find that there are two kinds of LSBs, "red" and "blue", with different star formation histories: the former are better described by a "faded disk" senario, while the latter are described by models with low, roughly constant star formation rate. According to our senario, these different routes are dictated simply by the galaxy's mass, which induces an earlier SFR in the former case (because of the more rapid infall). A clear prediction of our models is that "blue" LSBs should be less massive and less luminous than the "red" ones.

The observational implications of colour and photometry profiles and their relationship to abundance gradients (not presented here) is postponed to a forthcoming paper (Boissier and Prantzos, in preparation).

3.4 Integrated present day properties

Assuming that all our model disks started forming their stars ∼13 Gyr ago, we present in Fig. 8 their integrated properties today (at redshift z=0). Several interesting results can be pointed out:

1) For a given λ, the stellar and gaseous masses are monotonically increasing functions of V_C. For a given V_C disks may have considerably different gaseous and stellar contents (by factors 30 and 5, respectively), depending on how "compact" they are, i.e. on their λ value. The more compact galaxies have always a smaller gaseous content. This is well illustrated by the behaviour of the gas fraction σ_g(*bottom left* of Fig. 8). There seems to be a rather good correlation between σ_g and V_C for all λ values, a feature that is indeed observed (see Sec. 4.4). The most compact galaxies have always σ_g lower than 0.1, while the most extended ones (those corresponding to the LSBs discussed in the previous section) have always σ_g >0.5. The latter property seems indeed to be an observed feature of LSBs (McGaugh and de Blok 1997, and Sec. 4.4). In general, the final gas fraction is a slowly decreasing function of V_C and a rapidly increasing function of λ.

2) The pattern of the average oxygen abundance (i.e. total oxygen mass in the gas, divided by the gas mass, *central pannel* in Fig. 8) can be readily understood on the basis of the behaviour of the gas fraction: wherever the latter is low (see point 1) the metallicity is high. Most of our models have average metallicities lower than solar. Only the most massive and compact ones develop average metallicities larger than 2 times solar. Our LSB candidates have average metallicities ∼0.5 solar.

3) The total SFR presents an interesting behaviour (*middle bottom pannel*): the current SFR Ψ_0 is found to be mostly a function of V_C alone, despite the fact that the amount of gas varies by a factor of ∼2-3 for a given V_C. This is due to the fact that more extended disks (higher λ) are less efficient in forming stars, because of the $1/R_d$ factor (for a given V_C). This smaller efficiency compensates for the larger gas mass available in those galaxies, and a unique value is obtained for Ψ_0. This immediately implies that little scatter is to be expected in the B-magnitude vs. V_C relation, and this is indeed the case as can be seen in Fig. 8 (*middle right pannel*). The λ=0.01 case does not follow this pattern, since very little gas is left in the disk; as stressed on several occasions, this case corresponds rather to bulges or elliptical galaxies and is shown here only as a limiting case of our disk models. The implications for the Tully-Fisher relation are discussed below (Sec. 4.2).

4) The mass to light ratio $\Upsilon = M/L$ is a quantity often used to probe the age and/or the IMF of the stellar population and the amount of dark matter, but also to convert results of dynamical models (i.e. mass) into observed quantities (i.e. light in various wavelength bands). From disk dynamics of high surface brightness galaxies Bottema (1997) inferred Υ_B=1.79±0.48 (for a Hubble parameter h=0.75). Using the value of $B-I$=1.7 for typical disk galaxies given by McGaugh and de Blok (1997), MMW98 derived Υ_I=(1.7±0.5)h, where the Hubble parameter H_0 = 100 h km/s/Mpc.

Our model values for Υ_B and Υ_I are plotted in Fig. 8 (*middle upper pannel*) along with the corresponding observational range (*grey bands*). It can be seen that: a) both Υ_B and Υ_I model values are slowly decreasing functions of V_C and slowly increasing functions of λ; b) most of the model values lie well inside the observationnaly derived range; c) the λ=0.01 case lies outside the observed range of Υ_B (another indication that this value of the spin parameter does not produce realistic disks).

In summary, our models lead to fairly acceptable values of Υ_B and Υ_I, these values are confined to a relatively narrow range and a systematic (albeit weak) trend is obtained with galaxy's mass, that should not be neglected in detailed models.

5) As discussed in Sec. 3.3, the central surface brightness μ_{B0} depends little on V_C, but quite strongly on λ. This can be qualitatively understood from Eq. (15) implying for the central surface density a strong dependence on λ, but a mild one on V_C. Taking into account that the λ-distribution peaks around 0.04-0.05 (MMW98) we see that most of our model disks have a roughly constant current μ_{B0} ∼21.5 mag arcsec^{-2}. This is quite an encouraging result, in view of the observed constancy of the central surface brightness in disks, around the "Freeman value" μ_{B0}=21.7±0.3 mag arcsec^{-2} (Freeman 1970); this value is indicated by the grey band in Fig. 8 (*top right pannel*). In the next section we show that the obtained values of central surface brightness in longer wavelengths are also in fair agreement with recent observational results. Finally, models with λ=0.07 and 0.09 result in LSB galaxies today (but not always in the past, see the discussion in Sec. 3.3).

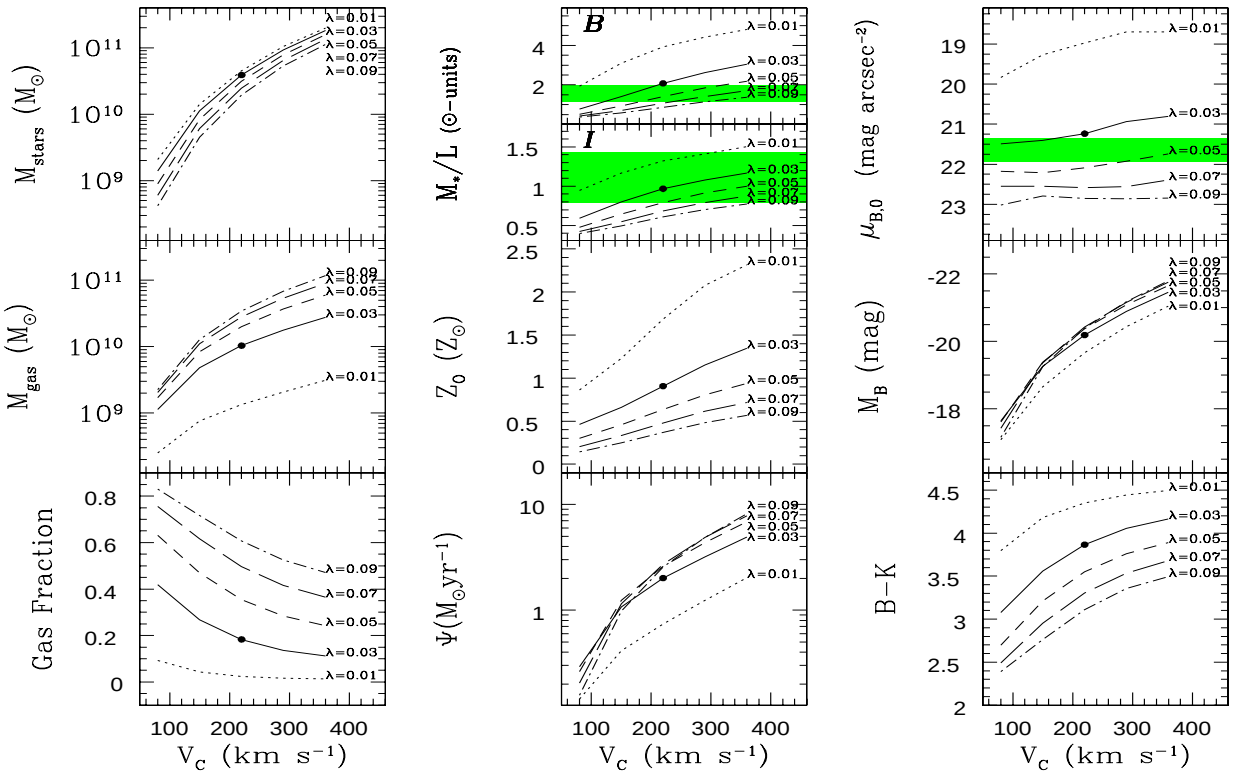

Figure 8. Integrated properties of our models at an age T=13.5 Gyr. Mass of stars (*top left*), mass of gas (*middle left*), gas fraction (*bottom left*), M/L values in B- and I- bands (*top center*), average oxygen abundance, i.e. total mass of oxygen divided by total mass of gas in the disk (*middle center*), star formation rate (*bottom center*), central surface brightness μ_{B0} (*top right*), total B-magnitude (*middle right*), total B-K (*bottom right*). All results are plotted as a function of the rotational velocity V_C and parametrised with the values of the spin parameter λ. The *filled symbols* on the λ=0.03 curves and for V_C=220 km/s in all pannels correspond to Milky Way values; as stressed in Sec. 2 the Milky Way is used to calibrate all our models, through the adopted scaling relations (eqs. 14 and 15). The *grey bands* in the M/L and μ_{B0} pannels indicate the corresponding ranges of observed values (see Sec. 3.4, points 4 and 5).

6) The final B-K colours of our models (Fig. 8, *bottom right pannel*) can also be readily understood by an inspection of the gas fraction pattern: for a given λ, more massive disks have less gas and are redder, while for a given V_C more extended disks (larger λ) have more gas and are bluer. Overall, the less massive galaxies have B-K values in the 2.5-3 range, while for the most massive ones we obtain values around 3.5-4.

4 RESULTS VS OBSERVATIONS

Having described in the previous section the main results of our models in terms of the input parameters V_C and λ, we turn now to a comparison of these results to observations. Our purpose is to check whether the results of our grid of models (a) bracket reasonably well the range of observed values of various galactic properties and (b) reproduce some observed strong correlations. Such a comparison is, in principle, possible if the age of the observed galaxies is known, but this is unfortunately not the case. We shall make then the assumption that all galaxies started forming their stars at the same epoch, around 13 Gyr ago. It is not *a priori* obvious whether this assumption is reasonable or not, but we shall see that in most cases it leads to quite acceptable results. In any case, as stressed in Sec. 3.1 the term "time of formation" is a rather loose concept for models with infall: the "effective" timescales for the formation of the stellar populations in our models are given in Fig. 5.

4.1 Boundary conditions: Disk size and central surface brightness

As explained in Sec. 2.2, our model disks are described by the central surface density Σ_0 and scalelength R_d. These are related to the "fundamental" parameters V_C and λ (fundamental because they refer to the dark matter haloes) through the scaling relations (14) and (15), which allow to use the Milky Way as a "calibrator".

In this section we check whether this type of modelling produces present day disks with "reasonable" morphological properties. The central surface brightness and scalelength in the r-band represent fairly well the underlying stellar population and are less affected by uncertainties due to dust extinction. The behaviour of our models in shorter wavelengths is somehat different, but we postpone an analysis of the colour gradients of our models to a forthcoming paper.

In a recent paper, Courteau and Rix (1999) analyse two large data samples of more than 500 non-barred disk galax-

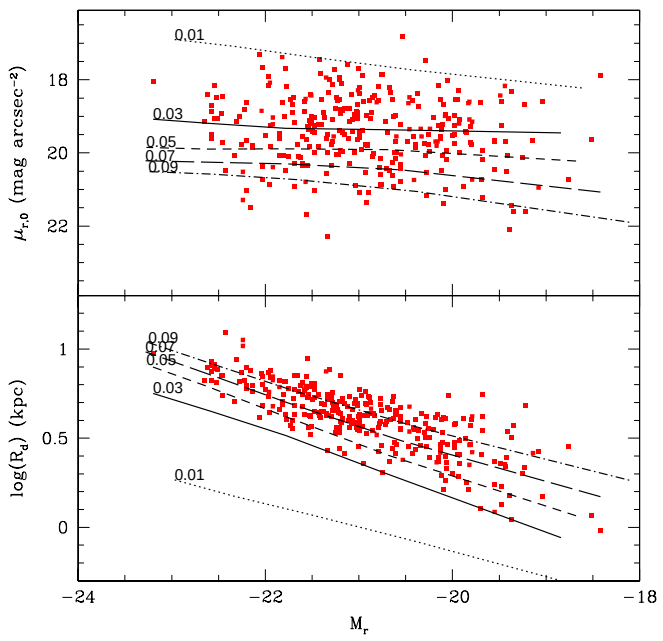

Figure 9. Central surface brightness (*upper pannel*) and disk size R_d (*lower pannel*) in the r-band, as a function of the galaxy's magnitude M_r. Our results are parametrised by the values of the spin parameter λ; λ=0.01 models produce unrealistically small disks with very high surface brightness and correspond rather to galactic bulges. Data are from Courteau and Rix (1999).

ies. They find that only ∼20% of these disks can be described by purely exponential profiles and they provide disk sizes, rotational velocities, magnitudes and colours. Their data allow to derive the central disk surface brightness.

In Fig. 9 we present the r-band central surface brightness (upper pannel) and size (lower pannel) of our model disks as a function of the galaxy's luminosity and we compare them to the data of Courteau and Rix (1999). It can be seen that:

i) The central surface brightness in our models compares fairly well to the data. For a given value of λ, μ_{r0} is quasi-independent on luminosity (or V_C), as explained in Sec. 3.4. The obtained values depend on λ, the more compact disks being brighter. All the observed values are lower than our results of λ=0.01 models. Higher λ values bracket reasonably well the data.

ii) The size of our model disks decreases with decreasing luminosity, with a slope which matches again the observations fairly well. Our disk sizes range from R_d ∼6-10 kpc for the most luminous galaxies to 1-2 kpc for the less luminous ones. The λ=0.01 curve clearly lies too low w.r.t. all data points, showing once more that it does not produce realistic disks.

It should be noticed that a similar comparison between theory and observations is made in MMW98. However, for lack of an evolutionary model, MMW98 compare rather the profiles of their gaseous disks (i.e. those given by our eq. 12 and 13) to the data, making the implicit assumption that gas is transformed into stars with the same efficiency in all parts of all disks. Our models show that this is a good approximation for the inner regions, but not for the outer ones

	a (slope)	b (0-point)	σ (scatter)
Observations			
Giovanelli et al.	7.68	-21.93	0.35 mag
Tully et al.	8.17	-21.54	0.42 mag
Han & Mould	7.87	-21.42	0.40 mag
Mathewson	6.80	-21.72	0.43 mag
Our models			
λ=0.01	6.81/7.17	-21.34/-21.70	
λ=0.03	7.01/7.31	-21.47/-21.72	
λ=0.05	7.37/7.71	-21.35/-21.54	
λ=0.07	7.79/8.10	-21.16/-21.30	
λ=0.09	8.18/8.44	-21.00/-21.05	

Table 1. The Tully-Fisher relation in the I-band: observations vs. our models (see Sec. 4.2 for references). A value of h=0.65 is assumed for the Hubble parameter in this Table and Fig. 10. Two values (separated by /) are given for our models: the first one corresponds to models with extinction taken into account and the second to models with extinction neglected. Observational data are from Giovanelli et al. (1997), Tully et al. (1998), whereas the Han and Mould and Mathewson et al. data are taken from the compilation of Willick et al. (1996).

(because of the adopted radial dependence of the SFR efficiency) and that the final stellar disk sizes are shorter than the initial gaseous ones. Moreover, MMW98 adopt a M/L ratio (the same for all disks) in order to convert their mass surface density to surface brightness. As discussed in point 4 of Sec. 3.4, the $\Upsilon = M/L$ ratio is a slowly increasing function of a galaxy's mass (at least accordingly to our models). Our self-consistent chemical and spectrophotometric evolution models allow to avoid these approximations and to compare directly the output to observations.

4.2 Dynamics: the Tully-Fisher relation

The Tully-Fisher (TF) relation is a strong correlation exhibited by the whole population of disk galaxies. It relates their luminosity L (or magnitude M) and their circular velocity V_C (or H_α line width W) and can be expressed as M= $-a\,[log(2V_c) - 2.5] + b$ or $L \propto V_c^{a/2.5}$. The exact slope of the relation and its zero point are still the subject of considerable debate (e.g. Giovanelli et al. 1997). For this reason, we compare our results with several recent fits to the I-band Tully-Fischer relation obtained with various data samples.

In a recent study, Giovanelli et al. (1997) compiled a homogeneous set of I-band photometry and HI velocity profiles of 555 spiral galaxies in 24 clusters with redshift extending to cz ∼9000 km/s. The slope of their TF relation is 7.68 ± 0.13. They estimate the mean amplitude of the scatter in the observed relation to be 0.35 mag, but they notice that it increases with decreasing velocity. They also estimate that the combination of statistical and systematic uncertainties can affect the zero point of the relation up to 0.07 mag, i.e. a rather small effect. In order to compare our results to the Giovanelli et al (1997) sample we shall assume that $h = 0.65$ i.e. a value very close to the $h = 0.69 \pm 0.05$ value derived by these authors on the basis of their data.

Willick et al.(1996) have computed several TF relations on the basis of samples from various authors. Two of those samples are in the I-band and shall be used in the present work. The first one is a cluster sample from Han, Mould

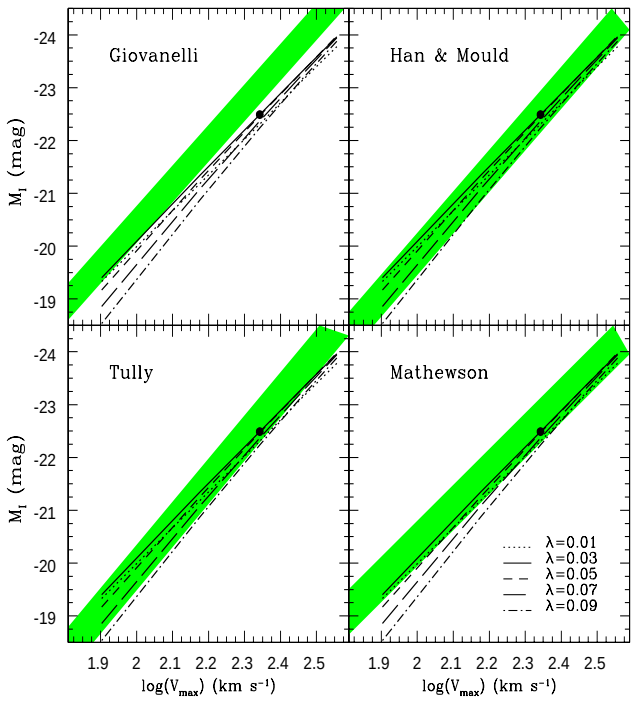

Figure 10. The Tully-Fisher relationship in the I-band. In each pannel, our results (*curves* parametrised by the corresponding λ value, as indicated in the *bottom right* pannel) are compared with fits from various authors (*shaded zones*), differing by their zero-points and slopes (see Table 1 and Sec. 4.2 for references on the data). The models shown here are those with extinction taken into account (first column in Table 1), which lead to flatter TF relations than when extinction is neglected. In all cases (except for Tully et al. 1998) the data are plotted assuming that the Hubble parameter h=0.65.

and coworkers (references are given in Willick et al.(1996)). They find a slope $a = 7.87\pm$ 0.16 and a scatter of 0.4 mag. The second one is the field galaxies sample of Mathewson et al. (1992), composed of 1219 galaxies. It provides a slope $a = 6.80\pm$ 0.08 and a scatter of 0.43 mag. For these two samples Willick et al.(1996) define the "Hubble absolute magnitude" of a galaxy, computed from its apparent magnitude and redshift and independent of the Hubble parameter; the zero-points of the TF relation are then determined through this Hubble absolute magnitude. In order to plot those two relations on a common scale with other samples, we transformed the quoted "Hubble absolute magnitudes" into usual absolute magnitudes by assuming h=0.65.

A fourth work (Tully et al.(1998)) uses a limited sample of 87 galaxies from the Ursa Major and Pisces Clusters. The obtained slope is steeper than in the other determinations (a=8.17) while the scatter is similar (0.42 mag). In that work, TF relations in other photometric bands (B,R,I,K') are considered for the same galaxy sample; we shall compare them to our results in the end of this section.

The parameters of those various fits are presented in Table 1, and the data are compared with our models in Fig. 10. It can be seen that:

a) The model slopes and zero-points depend somewhat on λ: in general, larger λ values lead to steeper M-V_C relations. This is is due to the following reason: At high V_C all galaxies transform most of their gas into stars, i.e. the final stellar mass depends little on λ and so is the case for the corresponding M$_I$. As we go to lower V_C, the final stellar mass depends more and more on λ, because higher λ galaxies are more inefficient in forming stars: this is reflected in a steeper slope of the corresponding M-V_C relation.

b) Since the most probable values of λ are in the 0.04-0.05 range (according to numerical simulations), our corresponding slopes of the M-V_C relation are a ∼7.1-7.3 (with extinction taken into account). This value of a is intermediate between those obtained from the samples of Giovanelli et al., Mathewson et al. and Han, Mould and collaborators. It is certainly lower than the slope in the Tully et al. sample, which concerns, however, disk galaxies in clusters; in such environments disks probably evolve quite differently than in the field, being affected by interactions. Our models are better compared to field galaxies, such as those in the sample of Mathewson et al.

c) Because of the very inefficient star formation at low V_C and high λ, the TF relation of our models shows a magnitude dependent scatter, from ∼0.1 mag at high V_C to ∼0.5 mag at low V_C. This trend is not apparent in the observed relations appearing in Fig. 10 (*shadowed zones*), since only the average scatter appears. However, Giovanelli et al. (1997) find that there is indeed a trend of increasing scatter with decreasing magnitude in the TF relation. Notice that in our models, the galaxies that contribute mostly to that scatter at low V_C are the low surface brightness galaxies (λ ∼0.07-0.09); such galaxies are, in general, not included in the observed samples. In any case, a clear prediction of our models is that the scatter in the TF relation should be more important at low V_C.

d) Extinction modifies somewhat the slopes, leading to slightly swallower TF relations than those obtained by the stellar population alone. This is because it affects more the massive (high surface brightness and high metallicity) disks, rather than the low mass ones. If our extinction values are overestimated, then the slopes of our models should be intermediate between the two values given in Table 1. This is also true for the zero-points.

It should be noticed here that, if the initial gas were almost completely turned into stars, one should naturally expect a $L \propto V_C^3$ relation (from Eq. 4, assuming $m_d = const$ and $M/L = const$). In other words, the adopted scaling relations lead to a "built-in" TF relation, as properly pointed out in MMW98. However, when star formation is properly taken into account in "realistic models", different slopes are found, depending on the SFR efficiency (itself a function of λ, see Table 1). Although the differences introduced by the more realistic senarios are relatively small, they may have important implications for a proper interpretation of the TF relation. In particular, our models, taken at face value, suggest that low surface brightnesss galaxies (i.e. those with λ >0.07) should have steeper TF relations than those of high surface brightness in the I-band.

Tully et al. (1998) also investigated the slope of the TF relation in several wavelength bands. They found that the slope increases with wavelength, as can be seen in Table 2. Our results are also shown on Table 2 and in Fig. 11,

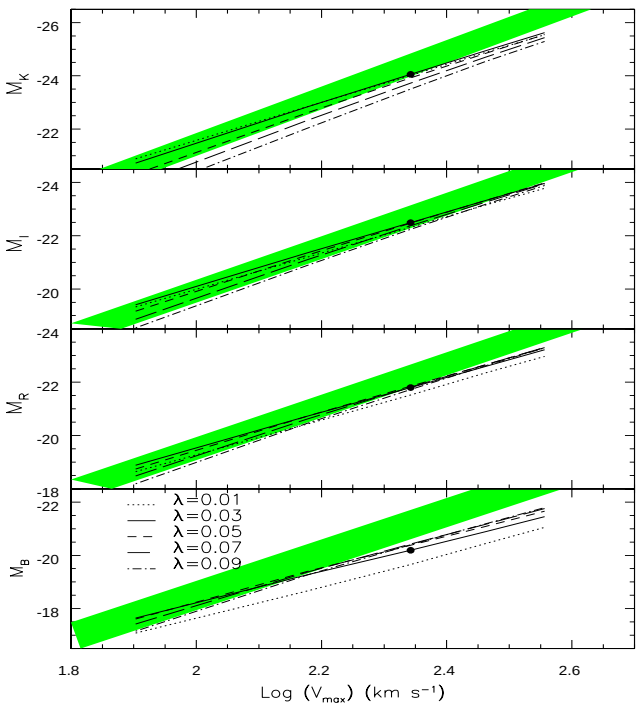

Figure 11. The Tully-Fisher relationship in several photometric bands. Our results (*curves* parametrised by the corresponding λ value, as indicated in the *bottom* pannel) are compared with the Tully et al.(1998) observations (shaded zones).

Photometric band	λ =0.01	0.03	0.05	0.07	0.09	Observed (Tully)
B	6.1	5.8	6.2	6.6	7.1	*7.79*
R	6.7	6.7	7.0	7.4	7.9	*7.96*
I	6.8	6.9	7.3	7.8	8.2	*8.17*
K'	7.1	7.5	8.0	8.4	8.8	*8.73*

Table 2. Slopes in the TF relations $L_\lambda \propto V_c^{a/2.5}$, in various wavelength bands. Our models (arranged by λ values) are compared to the observations of Tully et al. (1998); see also Fig. 11.

compared to the observational fits of Tully et al. (1998). The following points should be noticed:

i) In our models, the trend of increasing slope with increasing λ is found in all wavelength bands, not only in the I-band.

ii) As we go from the B- to the K'-band, our models do predict a steeper and steeper slope for all λ values. Leaving aside the λ=0.01 case (unrealistic for disks) one sees that the slope a increases between B- and K'-bands by $\sim$1.8 for all λ values. This increase is somewhat larger than the corersponding increase of $\sim$1 in the data of Tully et al. (1998).

iii) Our model values for the slope a are, in general, smaller than those of Tully et al. (1998), especially in the B-band. Only the λ=0.09 models lead to values comparable to those of Tully et al. (1998) in the R, I and K' bands.

As stressed already, the Tully et al. (1998) data concern spirals in clusters which cannot be directly compared to those modelled in our work; our slopes in the I-band compare rather well to the field galaxy sample of Mathewson et al. But the important issue here is the trend of *increasing slope* with wavelength, found in both theory and observations. In our models this increase is due to the fact that less massive galaxies are chemically and photometrically "younger" than their more massive counterparts, having in general "bluer" colours. This is shown in Fig. 8 (*bottom right* pannel), where B-K increases systematically with V_C. This change in B-K with V_C produces a steepening in the slope of the TF relation as we go from the B- to the K-band. This feature is not "built-in" in our models (it does not stem directly from the adopted scaling relations) but it results from the adopted prescription for the SFR *and* the infall rate (Sec. 2.3), making less massive galaxies appear "younger" than more massive ones. This generic feature of our models is crucial also in interpreting the metallicity-luminosity relation of disks (see Sec. 4.5) and we consider it to be one of the most important points of this work.

In a recent paper, Heavens and Jimenez (1999) use also semi-analytic disk models in CDM senarios and a rather simple prescription for star formation in order to investigate the variation of the slope of the TF relation with wavelength. They apparently manage to reproduce the oberved trend, but they offer no explanation for their success. They also suggest that λ value and formation redshift z are the parameters that can explain the observed dispersion in the TF relation. Our models show that this is certainly true for λ, but the disk baryonic fraction m_d (taken as constant here) could obviously play a similar role.

4.3 Luminosity evolution: Colour-colour and colour-magnitude relations

Spectro-photometric models are usually calibrated on colour-colour and colour-magnitude diagrams. The parameters of the models (star formation efficiency, stellar IMF, infall time-scales, ages ...) are chosen as to reproduce the properties of galaxies of all morphological types (e.g. Lindner et al.(1999), Fioc & Rocca-Volmerange(1997)).

As explained in the Introduction, our study is limited to the case of spiral galaxies, because they offer a much larger amount of observational data to compare with. However, we have not "tuned" any parameters in order to reproduce any diagram of this kind. It is thus of interest to see if our models, generalized from the Milky Way by the use of simple scaling relations, are able to reproduce those diagrams for spiral galaxies. For this aim, we used data from De Jong, 1996. De Jong's data consists in radial and integrated photometry of 86 undisturbed face-on spirals. They are thus directly comparable to our models, since uncertainties due to inclination, or to perturbations by nearby galaxies (which could have affected the star formation activity) are avoided. We evaluated the disk magnitudes and colours in de Jong's sample by using his fits for the disks only (i.e. central surface brightness and disk scalelength) and plot them on Fig. 12 (notice that the error bars reflect the uncertainties of the fit, not those of the observations).

Since the age of the observed galaxies is not known, we show in Fig. 12 our results for three different epochs: t=3, 7.5 and 13.5 Gyr, covering the expected range of galaxy ages. It is clearly seen that:

1) At all ages there is a tight $B-K$ vs $B-V$ corre-

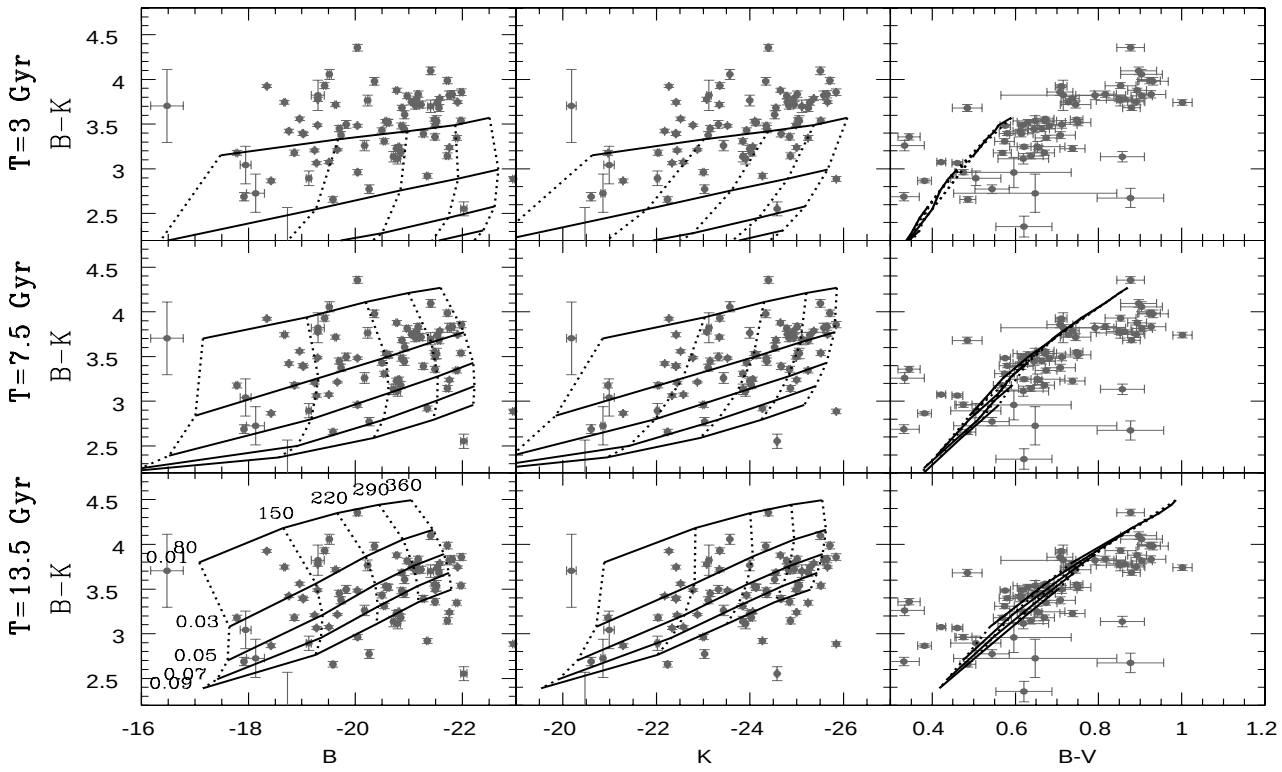

Figure 12. Colour-magnitude and colour-colour relations for our models at three different ages: 3 Gyr (*upper pannels*), 7.5 Gyr (*middle pannels*) and 13.5 Gyr (*lower pannels*). The grid of models represents 5 values for the spin parameter λ (0.01 to 0.09 from *top to bottom* in *solid curves*) and 5 values for the circular velocity V_C (80 to 360 km/s from *left to right*, in *dashed curves*), arranged as indicated in the lower left pannel. In the $B-K$ vs $B-V$ relation our grid is "squeezed" onto a relatively tight relation, determined mainly by V_C. Data in all pannels (the same points are plotted in each row) are from de Jong (1996). We have calculated magnitudes and colours for *disks only*, using de Jong's fits (central surface brightness and disk scalelength). Clearly, the observed galaxies are older than 3 Gyr, and rather closer to 13.5 than to 7.5 Gyr.

lation, quasi-independent of the value of λ. It depends only on the galaxy's mass (i.e. luminosity): lower mass galaxies are always "bluer" than more massive ones.

2) Results at t=3 Gyr do not compare well to the data: model disks are too blue. The observed galaxies cannot be as be as young as 3 Gyr.

3) At t=7.5 Gyr the results compare much better to the data, although there is still a lack of "red" model galaxies (i.e. with $B-V$ in the 0.8-1.1 range).

4) At t=13.5 Gyr the agreement between theory and observations is quite satisfactory. The observed colours and magnitudes are well bracketed by our grid of results.

5) Our models do predict a colour-magnitude relation which becomes steeper with time. More luminous galaxies are "redder" on average (as can also be seen on Fig. 8, *bottom right*). De Jong's data support this picture qualitatively. Also, the slope of the B-K vs. B-V relation (*bottom right pannel* in Fig. 12) depends little on λ or V_C; it is slightly steeper than the observed one, but the overall comparison is fairly satisfactory.

It is obviously difficult to assign an "age" to these galaxies on the basis of such diagrams. Increasing slightly the efficiency of star formation in Eq. (1) would lead to similar results at ages lower by a few Gyr. Further constraints should be considered, like those analysed in the next sections.

We wish to emphasize here the fact that our adopted senario (infall and star formation timescales longer for low mass galaxies) leads naturally to the trend of massive galaxies being "redder" on average, as observed. This trend is a well-known problem in hierarchical models of galaxy formation, where low mass galaxies are formed first and are found to be "redder" today than massive ones. In their recent work Somerville and Primack (1998) suggest that this problem may be overcome by including in the models dust extinction, which affects more the massive galaxies and makes them "redder" on average. However, in our models we find that dust extinction plays a minor role: it can modify slightly the situation (enhancing the already existing trend in the stellar population alone) but not reverse it completely. And is certainly not dust extinction that makes the Milky Way appear chemically and photometrically older than the Magellanic Clouds.

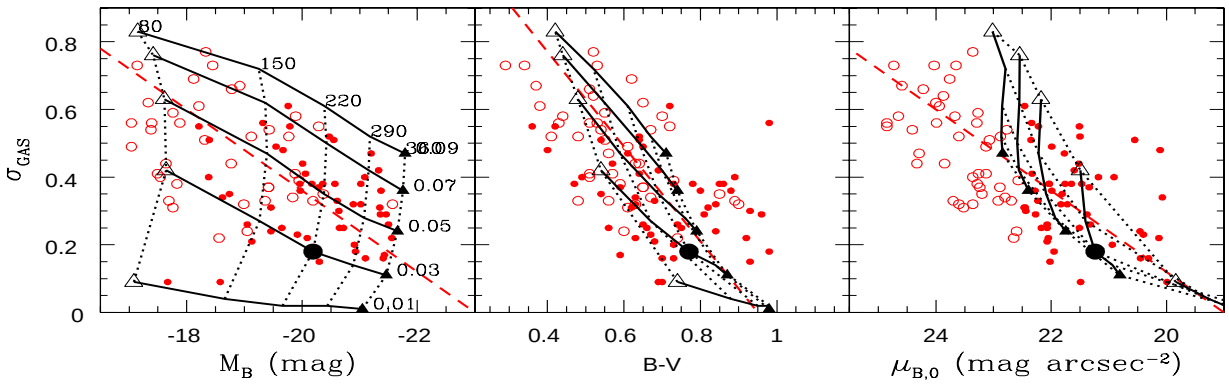

Figure 13. Gas fraction vs. B-magnitude (*left pannel*), B-V colour (*middle pannel*) and central surface brightness μ_{B0} (*right pannel*). The grid of models represents 5 values for the spin parameter λ (*solid curves*) and 5 values for the circular velocity (*dashed curves*), as indicated on the left pannel. Values of V_C run from 80 km/s (*open triangle*) to 360 km/s (*filled triangle*). Results of models are given at a galactic age of 13.5 Gyr. Data in all pannels are from McGaugh and DeBlok (1997). *Filled symbols* correspond to high surface brightness galaxies and *open symbols* to low surface brightness galaxies. Our grid of models clearly does not fit the lowest surface brightness galaxies (i.e. below μ_{BO}=23 mag arcsec^{-2}), which probably require values of λ >0.1. In all three pannels, the *dashed* diagonal line is a fit to the data given in McGaugh and DeBlok (1997): σ_g = 0.12 (M_B+23) = -1.4 [(B-V)-0.95] = 0.12 (μ_{BO}-19).

4.4 Chemical Evolution: Gas fraction vs. Magnitude and Colour

Diagnostics of galaxy evolution can be made in a variety of ways. Colour-colour diagrams are often used for that purpose, as discussed in the previous section. However, their usefulness is limited by the fact that they admit "degenerate solutions", i.e. "red" stellar populations may result either from old age and low metallicity or young age and high metallicity.

A key ingredient to galaxy evolution is the consumption of gas, turned into stars; as time goes on, the gas fraction σ_g decreases in general (except in cases where infall exceeds the star formation rate). The gas fraction could then, in principle, be used to probe the evolutionary status of galaxies.

This probe has rarely been used in studies of galaxy evolution up to now, for several reasons. First, it is also affected by "degeneracy": galaxies may have low gas fractions either because of quiescent star formation for a long time or because of recent enhanced star forming activity. Secondly, until recently, the observed range of values in σ_g was rather small (σ_g <0.2) and provided little constraints to models. It seemed indeed that we live at a special epoch, when most galactic disks have almost exhausted their reservoir of gas (e.g. Kennicutt et al. 1994).

In an important recent work McGaugh and deBlok (1997) compiled data from several surveys and derived various important quantities for galaxy evolution studies: colours, absolute magnitudes, scalelengths, central surface brightness, atomic and molecular gas amounts. On the basis of these data they were able to establish several important correlations between the gas fraction and other quantities, in particular B-V and B-I colours, absolute magnitudes and central surface brightness in the B- and I- band. On the other hand, they found no apparent correlation between gas fraction and disk scalelength. Another important finding of their work is that gas rich galaxies (i.e. with σ_g >0.4) do exist, but they are systematically low surface brightness galaxies.

In Fig. 13 we compare our results to the data of McGaugh and deBlok (1997). The following points can be made:

1) We find indeed a trend between gas fraction and absolute magnitude: smaller and less luminous galaxies are in general more gas rich, as can also be seen in Fig. 8 (*bottom left* pannel). Our grid of models covers reasonnably well the range of observed values, except for the lowest luminosity galaxies (see also points 2 and 3 below). In particular, the slope of the σ_g vs. M_B relation of our models is similar to the one in the fit to the data given by McGaugh and deBlok (1997). Moreover, among our models, closest to this fit are those with λ=0.05 (and 0.04, if we interpolate to the next value of λ=0.03), i.e. the value near the peak of the λ-probability distribution that is obtained from numerical simulations.

2) We find that the observed σ_g vs. B-V relation can also be explained in terms of galaxy's mass, i.e. more massive galaxies are "redder" and have small gas fractions. Indeed, the slope of the σ_g vs. B-V relation (-1.4) is again well reproduced by our models, and the λ=0.05 models lead to results that match close the observations. However, although our grid of models reproduces well the observed dispersion in σ_g, it does not cover the full range of B-V values. The lowest B-V values correspond to gas rich galaxies ($\sigma_g \sim$ 0.5-0.8) and could be explained by models with higher λ values than those studies here (i.e. by very Low Surface Brightness galaxies). However, observed galaxies that are both "red" (B-V$\sim$1) and gas rich (σ_g >0.3) are difficult to explain in the framework of our models.

3) The situation is radically different for the σ_g vs. μ_{B0} relation. As already seen in Fig. 8 (*top right* pannel) we find no correlation in our models between μ_{B0} and V_C, but we do find one between μ_{B0} and λ: more compact disks (lower λ) have higher central surface brightness. It is this latter property that allows our models to reproduce, at least partially, the observed σ_g vs. μ_{B0} relation (*right pannel* of Fig. 13). It can be seen that for a given λ, similar values of μ_{B0} are obtained for all galaxy masses (or V_C), but when different

values of λ are considered, a large part of the observations in the σ_g-μ_{B0} plane is covered by our grid of models. Galaxies with high μ_{B0} (20-21 mag arcsec^{-2}) and low σ_g correspond to models with $\lambda \sim 0.02$. As in point 2 above, however, we are unable to reproduce galaxies with both high μ_{B0} and $\sigma_g >$ 0.3. On the other hand, our models do not reproduce very low surface brightness disks, with μ_{B0} >23 mag arcsec^{-2}; as explained in the previous paragraph, this is a rather minor problem, since such disks could result from models with $\lambda >0.1$, not considered here.

We should like to stress that it is the first time (to our knowledge) that a comparison of this kind of data is made to fully self-consistent models of chemical and spectrophotometric evolution of galaxies. Although the agreement between theory and observations is by no means perfect, it nevertheless suggests that the basic picture may be correct. The main result is that the σ_g vs. M$_B$ and σ_g vs. B-V relations can be explained in terms of galactic mass (or, equivalently, V_C), but the σ_g vs μ_{B0} relation can only be (partially) explained in terms of the spin parameter λ.

It is interesting to notice that in their work McGaugh and deBlok (1997) have speculated on these relations, on the basis of older, one-zone models of galaxy evolution (by Guiderdoni and Rocca-Volmerange 1987). In particular, they anticipated that the galaxy's baryonic mass may be the driving factor in explaining the σ_g vs. M$_B$ relation, as we find in our models. However, they suggested that the σ_g vs. μ_{B0} relation could be explained if low surface brightness galaxies are on the average 3-5 Gyr younger than the high surface brightness ones. Instead, we interpret the observed correlation in terms of λ, not of age differences. We are aware though that age is a third parameter that affects the results and may render the picture more complex than scetched above. We prefer, however, to keep a minimum of simplicity in our models and assume that all disks started forming stars at least 10 Gyr ago, unless there is compelling evidence for the contrary.

4.5 Chemical evolution: Metallicity vs. integrated and local properties

Metallicity is another probe of the evolutionary status of a galactic disk. Both its absolute value and its radial profile can be used as a diagnostic tool to distinguish between different models of galactic evolution.

Zaritsky et al. (1994) provided a sample of 39 disk galaxies for which oxygen abundances have been measured in at least 5 HII regions. They determined radial abundance profiles and deduced the oxygen abundance at three caracteristic radii: an absolute physical radius (at 3 kpc from the center) and two dimensionless radii, namely 0.4 ρ_0 (ρ_0 being the isophotal radius) and 0.8 ρ_s (ρ_s being the disk exponential scale-length, i.e. R_d in our notation). Zaritsky et al. (1994) found a strong correlation between the abundances at each of these radii and the disk circular velocity V_C, and a slightly weaker correlation between abundances and absolute magnitude M$_B$. They also found a correlation between abundances and Hubble type, but the fact that mass (i.e. V_C) and Hubble type are correlated with each other among spirals makes difficult to evaluate the role of the latter in shaping these correlations.

In Fig. 14 we plot our results at the same caracteristic

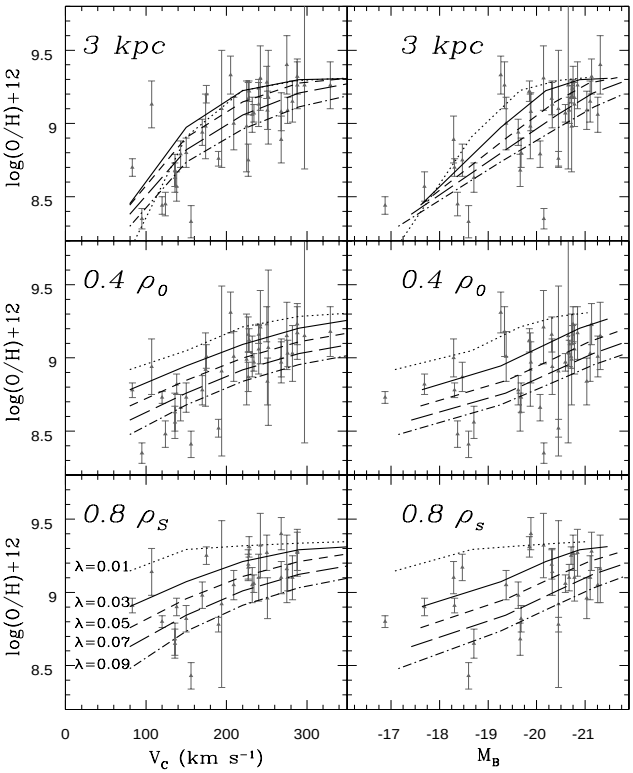

Figure 14. Oxygen abundances at various galactocentric distances: at 3 kpc (*upper pannels*), 0.4 ρ_o (*middle pannles*), and 0.8 ρ_S (*lower pannels*). They are plotted as a function of V_C (*left*) or, equivalently M_B (*right*). Our results (*curves*) are parametrised by the corresponding λ values. Data are from Zaritsky et al. (1994).

radii as Zaritsky et al. (at 3 kpc, at 0.4 ρ_0 and at 0.8 R_d, from *top* to *bottom*, respectively) as a function of circular velocity V_C (*left pannels*) and of M$_B$ (*right pannels*).

It can be seen that a correlation is always found in our models between abundances (Z) and V_C or M$_B$, stronger in the case of Z(3 kpc) than in the other two cases. Only in the λ=0.01 models (unrealistic for disks, as stressed already), Z(0.8 R_d) is not correlated with either M_B or V_C. Except for that, the grid of our models reproduces fairly well the data, both concerning absolute values and slopes of the correlations. Again, it is the first time (to our knowledge) that a detailed comparison of this type of data is made to fully self-consistent models of galactic chemical and photometric evolution. We think that the results of this comparison are quite satisfactory.

Zaritsky et al. (1994) point out that the trend of Z vs. M$_B$ observed in their galactic disks is simply the continuation of the abundance-luminosity relation noticed by Garnett and Shields (1987) over a wide range of magnitudes between spirals and irregulars. The relation spans over 10 magnitudes in M$_B$ and over a factor of 100 in metallicity. If galactic mass is always driving this relation (as in our models), then little room is left for galactic winds to play an important role; indeed, it is often claimed that low mass galaxies suffer loss of metals and/or gass through galactic winds, but in that case a deviation from the correlation ob-

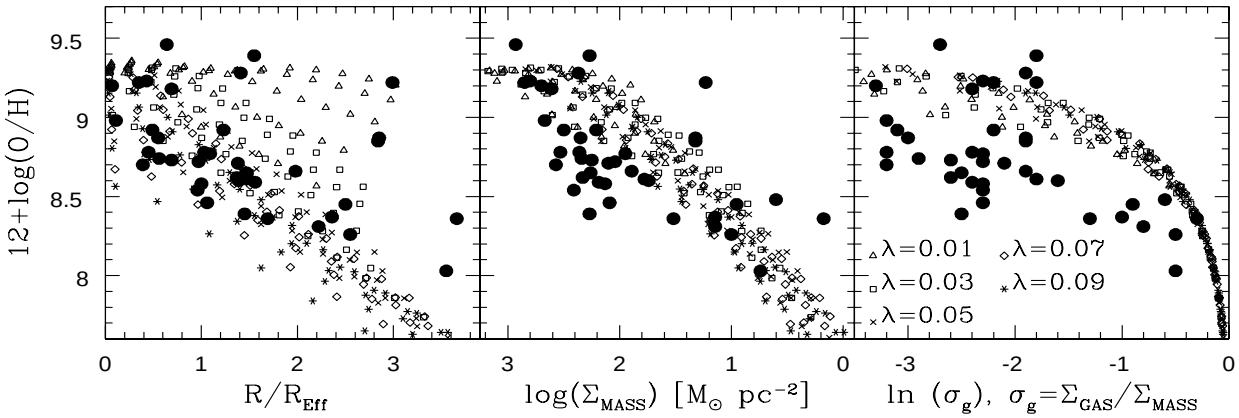

Figure 15. Oxygen abundances as a function of radius (in units of the effective radius R_{Eff}, *left pannel*), local surface density (*middle pannel*), and local gas fraction (*right pannel*). Our model results (*open sumbols*) are given at an age of 13.5 Gyr and correspond to different galactocentric distances; they are parametrised by the corresponding λ value, as indicated on the right pannel. Data (*filled symbols*) are from Shields et al. (1991) for HII regions in field spirals.

served in high mass galaxies (presumably unaffected by mass loss) would be expected.

It should be noticed that Zaritsky et al. (1994) find no correlation between metallicity and gas fraction σ_g in a limited sub-sample (14 galaxies) of their data. As shown in Fig. 8, we do find such a correlation in our results (higher Z for lower σ_g). However, this correlation is stronger for high σ_g, while at low σ_g (below $\sim$0.2) metallicity tends to "saturate". Zaritsky et al. (1994) admit that their negative result may be due to the fact that their sub-sample is limited to relatively low gas fractions. It is interesting to notice that our results show also that metallicity tends to saturate at a value of log(O/H)+12 $\sim$ 9.3 for the most massive disks, i.e. those with the lowest gas fractions according to Fig. 8.

The results of Zaritsky et al. (1994) concern abundances as a function of *global* galactic properties. Abundances in spiral galaxies as a function of *local* properties were studied by Shields et al. (1991), who searched for environmental effects between field and cluster galaxies (those in Virgo). They compiled data on abundances in HII regions and atomic and molecular gas surface densities as a function of galactocentric radius in five field galaxies. We concentrate on those field galaxies only, that presumably evolved "passively" (i.e. with no environmental effects) and correspond better to our models.

The data of Shields et al. (1991) are plotted in Fig. 15 and compared to our results. Oxygen abundances are plotted as a function of radius R (normalised to effective radius R_{Eff}), of total surface density Σ and of gas fraction σ_g. Our results are shown at an age of 13.5 Gyr, parametrised by the values of spin parameter λ. It can be seen that:

1) There is a good anti-correlation in general between metallicity and $R/R_{Eff}, \Sigma$ and σ_g (*left, middle* and *right* pannels, respectively). The scatter in the observed relation is larger in the case of Z vs. R/R_{Eff} and smaller in the case of Z vs. Σ.

2) Our models reproduce well, in general, the observed trends. However, the scatter in the observed Z vs. R/R_{Eff} relation is only reproduced when λ=0.01 models are considered: they are the only ones producing high metallicities at large R/R_{Eff}. But such λ values produce unrealistic disks, as stressed several times in this work ; and if we neglect them, we are unable to reproduce the observed scatter. The solution to that difficulty may reside in the fact that the large abundances at large R/R_{Eff} in the Shields et al. (1991) data come from only one galaxy, N2903. If this, perhaps "peculiar", galaxy is removed from the sample, the rest of the data present a tighter correlation that is readily explained by our models with $\lambda >$0.02.

3) The metallicity vs. surface density relation presents the tightest correlation, both observationally and in our models. We find an excellent agreement between theory and observations in that case.

4) The metallicity vs. gas fraction relation is the most intriguing. Our model results are systematically $\sim$0.2-0.3 dex higher than the observations. One might think that the adopted yields are too high by $\sim$50%; such an uncertainty in stellar yields is indeed conceivable (see Prantzos 1998). However, in that case our results as a function of R/R_{Eff} and Σ should also be modified: lowering the theoretically predicted O/H by 0.2-0.3 dex would spoil the excellent agreement with the data. Another possibility is that gas fractions have been systematically underestimated in Shields et al. (1991): moving the data points to the right (in the *right pannel* of Fig. 15) could alleviate the discrepancy. Also, a combination of those two factors (i.e lowering the theoretical metallicity and increasing the observed gas fraction) would help. We wish, however, to point out an interesting parallel with the situation in our own Galaxy. It has been noticed on several occasions (e.g. Pagel 1997) that solar CNO abundances are higher by 30-50% than those in nearby young stars and the local interstellar medium (ISM). Standard galactic chemical evolution models are usually required to reproduce solar abundances 4.5 Gyr ago and they always find present day CNO abundances larger by $\sim$30-50% than those observed in the local ISM (while reproducing correctly the present-day local gas fraction, see e.g. Prantzos and Aubert 1995). Our models being calibrated on the Milky Way, it is interesting

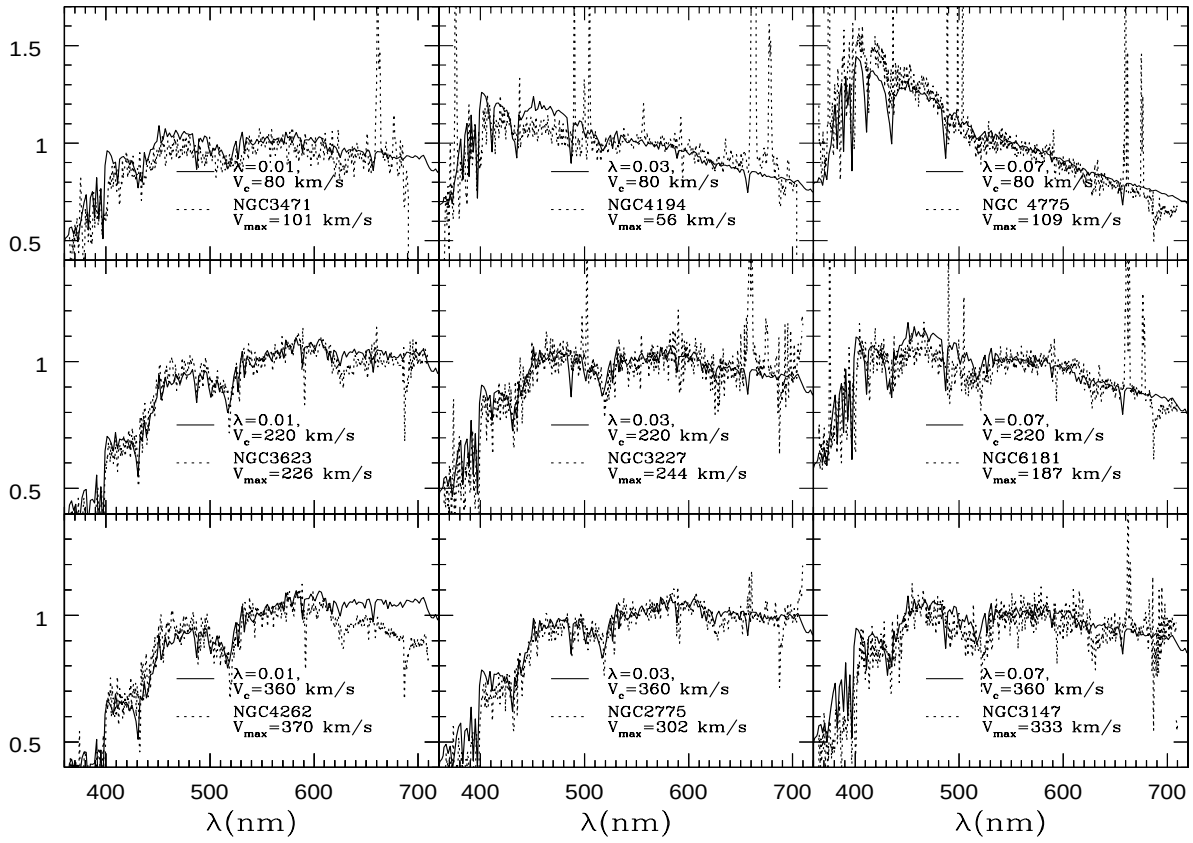

Figure 16. Spectra of our model disks at an age of T=13.5 Gyr, compared to observed spectra from the Catalogue of Kennicutt (1992). We have selected a few representative values of λ (0.01, 0.03, 0.07 from right to left) and of V_C (80, 220, 370 km/s, from top to bottom) and plotted the corresponding integrated galactic spectra at T=13.5 Gyr (*solid curves*). For each of these cases, we selected in Kennicutt's catalogue spectra of galaxies with measured rotational velocities (V_{max} in each pannel, following the galaxy's name) as close as possible to the model values; they are plotted in *dotted curves*. All spectra are normalised to the flux at 550 nm. Notice that our model spectra do not include emission lines.

to see that they overproduce also present day oxygen abundances in field spirals, and by similar amounts! This constitutes one more indication that solar abundances may not be representative of the local ISM 4.5 Gyr ago, as pointed out in several works (Prantzos et al. 1996, Clayton 1997). Confirmation of this would have major implications for galactic chemical evolution studies.

4.6 Spectral evolution: integrated spectra

We calculated the integrated spectra of our galactic disk models, according to the procedure presented in BP99. Our aim is to see whether our models can match reasonably well observed spectra of spiral galaxies.

In Fig. 16 we show our results for three values of λ (0.01, 0.03 and 0.07, from *left to right*) and three values of V_C (80, 220 and 360 km/s, from *top to bottom*) at an age of 13.5 Gyr (*solid curves*). As cen be seen, the form of the spectrum depends on both λ and V_C. Low values of λ and high values of V_C lead to old stellar populations and to a severe depression of the spectrum "bluewards" of 400 nm, due to an efficient early star formation (see Fig. 4 and 8).

We searched in Kennicutt's (1992) catalogue of galactic spectra galaxies with measured rotational velocities close to our V_C values. For each one of them we were able to find observed spectra that match reasonably well our theoretical ones (*dotted curves* in Fig. 16). This is the case, for instance, of the large spirals NGC2775 and NGC3147 (V_{max}=302 and 333 km/s, respectively, in the middle and righ bottom pannel of Fig. 15).

We stress that the successful comparison of observed spectra to our models proves nothing about the quality of the latter. Indeed, there are several ways to obtain spectra corresponding to young, intermediate and old stellar populations, and use of composite spectra alone is a poor diagnostic tool (especially if extinction has to be taken into account).

However, the comparison of models to observations made in Fig. 16 (the first ever made that involves measured rotational velocities), when combined to other probes of galactic evolution (all those discussed in the previous sections) constitutes a powerful tool of galaxy diagnostics. Indeed, it would be interesting to see, for instance, what are the values of gas fraction, chemical abundances, colours, magnitudes, disk scalelengths etc. for the observed galaxies of Fig. 16, and check whether they fit to the general scheme elaborated in this work. Also, it would be interesting to find

out what makes galaxies with similar V_{max} (like NGC3471 and NGC 4775) display so different spectra; our models suggest that spin parameter may be the answer. In any case, a detailed study of this kind requires as uniform a set of data as possible. Work is curently in progress in that direction (Boissier and Prantzos, in preparation).

5 SUMMARY

In this work, we present a comprehensive study of the chemical and spectrophotometric evolution of spiral galaxies, using multi-zone models. With respect to previous studies of that kind, our work presents the following important features:

- The fully self-consistent treatment of chemical *and* spectrophotometric evolution, with up-to-date, metallicity dependent, stellar input data.

- The use of a realistic stellar IMF, i.e. *measured* in the solar neighborhood (Kroupa et al. 1993), instead of the often used Salpeter IMF in the whole mass range; also, the radial dependence of the SFR (proportional to the rotation frequency $V(R)/R$, with realistic $V(R)$ profiles), based on theories of star formation induced by spiral waves in disks.

- The calibration of the model on the Milky Way disk (BP99), fixing the star formation efficiency which is *not a free parameter* for the other disk models.

- The use of simple "scaling laws" for the properties (sizes and surface densities) of other galactic disks, that are adopted as boundary conditions in our study; these scaling relations are based on currently popular models of galaxy formation, in the framework of Cold Dark Matter senarios and allow to describe disks in terms of two parameters: rotational velocity V_C and spin parameter λ.

The main results of our models may be summarised as follows:

i) The final gas fraction σ_g, M/L ratio, metallicity and colours depend on both λ and V_C. Disks of low λ (compact) and/or high V_C (massive) are formed earlier (in less than 6 Gyr) and are "redder" today than disks with other (λ, V_C) values.

ii) Some disk properties are found to be quasi-independent of V_C (like central surface brightness μ_0, in agreement with observations), while others are independent of λ (like e.g. current star formation rate Ψ_0, absolute magnitude M_B or colour-colour relation).

iii) High λ values (>0.07) lead to Low Surface Brightness galaxies (as already shown in previous works, e.g. Jimenez et al. 1998), while λ=0.01 leads to unrealistically small and bright disks.

iv) Due to the inside-out star formation scheme adopted here, profiles of surface brightness and colours flatten in time.

Comparison of our results to a large body of observational data leads to the following conclusions:

1) Disk size and central surface brightness are well reproduce by our models, implying that the adopted scaling laws produce "realistic" boundary conditions; only λ=0.01 values produce unrealistic results, ressembling more to galactic bulges than to disks.

2) The Tully-Fischer relationship is "built-in" in this type of models (i.e. through the scaling relations, which constitute the boundary conditions of the problem), but realistic senarios for star formation lead to small but important variations: in particular, our models predict a scatter increasing with decreacing circular velocity (a trend suggested by the data of Giovanelli et al. 1997) and a steeper slope in the I-band for low surface brightness galaxies. Also, we find that extinction by dust makes the TF relation flatter than in the case of the stellar population alone. Most importantly, our models naturally predict an increase in the slope of the TF relation with decreasing wavelength, resulting from the fact that less massive galaxies are chemically and photometrically "younger" than more massive ones; this trend is indeed observed (Tully et al. 1998).

3) Colour-colour and colour-magnitude relations are well reproduced with the adopted (Milky Way-type) star formation efficiency, provided the observed disks are more than ∼10 Gyr old. More massive disks are "redder" on average than low mass ones.

4) The relation of gas fraction to magnitude M_B, colour B-V and central surface brightness μ_{B0} is well reproduced. The trends in the former two correlations are driven by galaxy's mass (V_C), while in the latter by the spin parameter λ. Some of the observed low surface brightness galaxies require models with higher λ values than those studied here. Observed high surface brightness galaxies with large gas fractions (σ_g >0.3) cannot be explained by our models.

5) Metallicity is found to be well correlated to mass and luminosity, in fair agreement to observations. Also, it is correlated to local environment (radius, total surface density), again in agreement with observations. Our models show higher metallicity than observed at a given mass fraction, reminding of an analogous situation in the Milky Way disk. This "problem" may represent another clue against the usual assumption that the solar abundances are typical of the local ISM 4.5 Gyr ago.

6) Observed spectra of spirals with measured rotational velocities are well reproduced by our models, when comparable values of V_C are considered. The spin parameter λ can help to explain differences between galaxies with the same rotational velocity.

The agreement of our models to such a large body of observational data is impressive, taking into account the small number of free parameters. Indeed, the only really "free" parameter is the dependence of the infall timescale on galactic mass (Fig. 3), since all other ingredients have been fixed already by the calibration of the model to the Milky Way disk. Although it does not constitute a proof of the validity of the model, this success suggests nevertheless a coherent overall picture for the evolution of galactic disks, along the following lines:

- Baryonic gaseous disks form in non-baryonic haloes, with properties given by simple scaling relations of the Cold Dark Matter senario.

- Timescales for star formation in the disks depend mainly on their mass: massive disks form *earlier* the bulk of their stars and reach higher metallicities and B-V values than their low mass counterparts. This picture seems to contradict the idea that low mass haloes (and baryonic disks) form first. However, the timescale for assembling the baryonic gas need not be the same as the star formation time scale: low mass galaxies may assemble relatively rapidly, but require a very long time to turn their gas into stars. This

point is crucial, because we found that it allows to explain simultaneously three important observed features: the variation of the slope with wavelength band in the TF relation (Sec. 4.2, Fig. 11), the fact that more massive galaxies are on average "redder" than low mass ones (Sec. 4.3) and the metallicity-luminosity relation of Zaritsky et al. (1994, Fig. 14). It is important to notice that, the assumption of mass-dependent galactic winds could help explain the third feature, but not the first one.

- Star formation in disks takes place inside-out, producing steep early gradients in metallicity and colour profiles, that flatten at late times.

Several other predictions of this senario can be checked against observations. In a forthcoming paper (Boissier and Prantzos, in preparation) we show that the resulting abundance gradients are in agreement with observations. Moreover, the senario predicts little evolution of massive disks at late times (since most of the action takes place early on) and more important late evolution for low mass disks. The former point seems to be supported by observations of disk properties up to redshifts of $\sim$1 (Lilly et al. 1998).

REFERENCES

Baugh C., Cole S., Frenk C. & Lacey C., 1997, Galaxy Scaling Relations: Origins, Evolution and Applications, p. 52
Bell E., Bower R., De Jong R., Hereld M. & Rauscher B., 1999, MNRAS, 302, L55
Boissier S. & Prantzos N., 1999, MNRAS, 307, 857 (BP99)
Bruzual A. & Charlot S., 1993, ApJ, 405, 538
Charbonnel C., Meynet G., Maeder A. & Schaerer D., 1996, A&AS, 115,339
Calzetti D., Kinney A. & Storchi-Bergman T., 1994, AJ, 117, 492
Clayton D., 1997, ApJ, 484, L67
Cole S., Aragon-Salamanca A., Frenk C., Navarro J. & Zepf S., 1994, MNRAS, 271, 781
Contardo G. , Steinmetz M. & Fritze-Von Alvensleben U., 1998, ApJ, 507, 497
Courteau S. & Rix H.-W., 1999, ApJ, 513, 561
de Jong R., 1996, A&A Suppl., 118, 557
Fioc M. & Rocca-Volmerange B.,1997, A&A, 326, 950
Freeman K., 1970, ApJ, 160,811
Garnett D. & Shields G., 1997, ApJ, 317, 82
Giovanelli R., Haynes M., Da Costa L., Freudling W., Salzer J. & Wegner G., 1997, ApJ, 477, L1
Guiderdoni B., Hivon E., Bouchet R. & Maffei B., 1998, MNRAS, 295,877
Guiderdoni B. & Rocca-Volmerange B., 1987, A&A, 186, 1
Heavens A. & Jimenez R., 1999, MNRAS, 305, 770
Jimenez R., Padoan P., Matteucci F. & Heavens A., 1998, MNRAS, 299, 123
Kauffmann G., White S. & Guiderdoni B., 1993, MNRAS, 264, 201
Kauffmann, G. 1996, MNRAS, 281, 475
Kauffmann G., Nusser A. & Steinmetz M., 1997, MNRAS, 286, 795
Kennicutt R., 1992, ApJS, 79, 255
Kennicutt R., 1998, ApJ, 498, 541
Kennicutt R., Tamblyn P. & Kongdon C., 1994, ApJ, 435, 22
Kroupa P., Tout C. & Gilmore G., 1993, MNRAS, 262, 545
Lejeune T., Cuisinier F. & Buser R., 1997, A&AS, 125,229
Lindner U., Fritze-Von Alvensleben U. & Fricke K., 1999, 341, 709
Lilly S. et al., 1998, ApJ, 500, 75
Mathewson D., Ford V., & Buchhorn M., 1992, ApJS, 81, 413
Matteucci F. & Greggio L., 1986, A&A, 154, 279
McGaugh S. & De Blok W., 1997, ApJ, 481, 689
Mo H., Mao S. & White S., 1998, MNRAS, 295,319
Molla M., Hardy E. & Beauchamp D., 1999, ApJ, 513, 695
Navarro J., 1998, ApJ submitted (astro-ph9807084)
Navarro J. & Steinmetz M., 1997, ApJ, 478, 13
Navarro J., Frenk K. & White S., 1997, ApJ, 490, 493
Pagel B., 1997, "Nucleosynthesis and galactic chemical evolution", Cambridge UP
Prantzos N., 1998 in "Abundance Profiles: diagnostic tools for galaxy history", Eds. D. Friedli et al.,, ASP Conf. Series 147, p. 171
Prantzos N. & Aubert O., 1995, A&A, 302, 69
Prantzos N., Aubert O. & Audouze J., 1996, A&A, 309, 760
Prantzos N. & Silk J., 1998, ApJ, 507, 229
Renzini A. & Voli A., 1981, A&A, 94, 175
Schaller G., Schaerer D., Maeder A. & Meynet G., 1992, A&AS, 96, 269
Shields G., Skillman E. & Kennicutt R., 1991, ApJ, 371, 82
Somerville R. & Primack J., 1998, astro-ph/9802268
Steinmetz 1998, in "Dark Matter in the Universe, Eds. S. Bonometto et al., IOS Press, p. 174
Tully R., Pierce M., Huang J., Saunders W., Verheijen M. & Witchalls P., 1998, AJ, 115, 2264
White S. & Frenk C., 1991, ApJ, 379, 52
Willick J., Courteau S., Faber S., Burstein D., Dekel A. & Kolatt T., 1996, ApJ, 457, 460
Woosley S. & Weaver T., 1995, ApJ Suppl., 101. 181
Wyse R. & Silk J., 1989, ApJ, 339, 700
Zaritsky D., Kennicutt R. & Huchra J.,1994, ApJ, 420,87